Generalized Fractional Ambiguity Function and Its Applications

Peeyush Sahay, Izaz Ahamed Shaik Rasheed, Pranav Kulkarni, Shubham Anand Jain, Ameya Anjarlekar, P. Radhakrishna & Vikram M. G

Circuits, Systems, and Signal Processing

ISSN 0278-081X

Circuits Syst Signal Process
DOI 10.1007/s00034-020-01398-7

Springer

Circuits, Systems, and Signal Processing
https://doi.org/10.1007/s00034-020-01398-7

Generalized Fractional Ambiguity Function and Its Applications

Peeyush Sahay[1] · Izaz Ahamed Shaik Rasheed[1] · Pranav Kulkarni[1] · Shubham Anand Jain[1] · Ameya Anjarlekar[1] · P. Radhakrishna[2] · Vikram M. Gadre[1]

Received: 18 July 2019 / Revised: 15 March 2020 / Accepted: 18 March 2020

Abstract
The ambiguity function (AF) is an essential time-frequency analysis tool to analyze the radar waveform properties in radar applications. It can be used effectively and reliably to analyze properties like the peak-to-side-lobe ratio, time delay resolution, Doppler resolution and tolerance characteristic. However, it fails to analyze higher-order chirp waveforms and is unable to estimate their parameters. To solve this problem, a generalized time-frequency transform-based generalized fractional AF (GFAF) and generalized fractional Wigner–Ville distribution (GFWVD) are proposed. GFAF is also a generalization of the Fourier transform-based ambiguity function and the fractional Fourier transform-based ambiguity function. The uncertainty principle for GFAF and GFWVD is derived. Examples are presented to demonstrate the effectiveness of GFAF in analyzing cubic chirp waveforms and estimating parameters of multicomponent cubic chirps. The superiority of GFAF is demonstrated by comparing the mean square error to Cramer–Rao lower bound and high-order ambiguity function under different input-signal-to-noise ratio conditions. The robustness is demonstrated by comparing the signal-to-noise ratio gain to that of the time domain-matched filtering and other ambiguity functions. Finally, fourth-order parameters of a real bat echolocation signal are estimated.

Keywords Ambiguity function (AF) · Generalized time-frequency transform (GTFT) · Generalized fractional ambiguity function (GFAF) · Generalized fractional Wigner distribution function (GFWDF) · Time-frequency distribution (TFD) · Higher-order chirps

Extended author information available on the last page of the article

Published online: 11 April 2020

1 Introduction

The ambiguity function (AF) is a crucial time-frequency analysis tool to estimate signal parameters in radar applications. It can be used effectively and reliably to analyze radar waveform properties like the peak-to-side-lobe ratio, time delay resolution, Doppler resolution, and Doppler tolerance characteristic. In most of the radar, sonar, and biomedical applications, a chirp signal is transmitted to hit a target, and the reflected signal is received and estimated to know the characteristics of the radar target. The reflected signals represent the characteristics of the target, and they are higher-order chirps. Thus, there is a need to estimate the parameters of these received signals [2,4,14,17,30,42].

Many transforms have been proposed to estimate parameters of higher-order frequency-modulated signals based on computation complexity and parameter estimation accuracy. Some linear transforms have been proposed to estimate the parameter of higher-order chirps such as polynomial Fourier transform [14], local polynomial Fourier transform [20], polynomial chirplet transform, generalized parametric time frequency transform [50–52], generalized time-frequency transform [34–36], maximum likelihood estimator [5,13], quasi-maximum likelihood estimator (QML) [12], and QML with reduced coarse search method [39]. All these higher-order linear transforms give better parameter estimation accuracy, and they do not produce cross-terms during multicomponent signal analysis. However, even though higher-order parameter estimation is possible, computational complexity increases drastically with the increase in polynomial phase order.

Some nonlinear transforms have been proposed to reduce the computational complexity to estimate the parameter of higher-order chirp signal such as cubic phase function [13], linear canonical transform-based ambiguity function [7,48], linear canonical transform-based Wigner Ville Distribution (WVD) [33,41], unified Wigner ambiguity function [53,54], high-resolution time-frequency rate representation [56]. All these transforms are capable of estimating parameters with reduced computational complexity as compared to higher-order linear transforms. However, they produce cross-terms during multicomponent signal analysis. So, they are unable to give good estimation accuracy in low signal-to-noise ratio (SNR) conditions. A new AF based on LCT called generalized LCT (GLCT) has been developed and shown to have better performances in terms of SNR [40]. Sparse fractional ambiguity function further reduces the computational complexity of fractional Fourier transform-based ambiguity function [23]. Similarly segmented sparse discrete polynomial phase transform [22,24] and sparse cubic phase function-based methods [25] have been proposed to detect chirp parameters in low SNR conditions. However, all these transforms are capable of estimating parameters up to third-order polynomial phase signal only. These transforms [22–25], along with the results obtained in this paper could be used to provide a basis for generalizing these results to higher-order frequency-modulated signals.

Some higher-order nonlinear transforms have been proposed to estimate higher-order chirp parameters (phase order ≥ 3) such as higher-order ambiguity function (HAF) and polynomial WVD. These produce cross-terms during multicomponent signal analysis due to the nonlinear nature of transform. Each correlation or phase differentiation in HAF increases the SNR threshold by 6 dB and degrades parameter

estimation accuracy. To reduce cross-terms during multicomponent signal analysis, product higher-order ambiguity function (PHAF) and integrated generalized ambiguity function (IGAF), HAF-CPF have been proposed [4,38]. These higher-order nonlinear transforms are capable of estimating parameter up to some higher order in low SNR condition due to the use of multiple correlations. IGAF is accurate in the analysis of polynomial phase signals, but it is computationally intensive [40]. Furthermore, these higher-order nonlinear transforms can estimate only the polynomial phase signal.

The generalized time-frequency transform (GTFT) has been shown to analyze any higher-order polynomial chirp signals [34–36]. In this paper, the GTFT-based GFAF and GFWVD is proposed to analyze a large variety of multicomponent frequency-modulated signals with reduced computational complexity. GFAF follows the property of index additivity of angle (similar to fractional Fourier transform (FrFT)-based AF). Hence, GFAF is computationally efficient. GFAF can analyze a variety of signals by appropriate selection of the parametric function in the GTFT kernel. Furthermore, GFAF with the appropriately selected kernel can be used to analyze or estimate parameters of hybrid sinusoidal frequency-modulated polynomial phase signals. GFAF estimates cubic chirp parameters with reduced computational complexity because of a single correlation. GFAF is capable of analyzing radar waveform properties; hence, it is useful in radar applications. GFAF provides better SNR threshold as compared to high-order ambiguity function (HAF), and other multi-lag phase differentiation transforms due to the use of a single correlation. A combination of correlation and higher-order GTFT kernel in GFAF can be used to analyze any higher-order chirp with reasonable computational complexity. The computational complexity of GFAF is lesser than generalized CPF, maximum likelihood, and QML estimator for estimating higher-order chirp parameters. These properties make GFAF superior to other transforms.

Parameter estimation of complex systems such as hydraulic systems as in [26] is a difficult problem. For estimating higher-order chirps with more parameters, specific meta-heuristic algorithms like the ones proposed in [27] and [44] can be explored to estimate parameters with reduced computation complexity. The parameter estimation done in this paper uses a nested linear search. However, due to a smaller number of parameters considered in cubic chirps, both types of algorithms are feasible.

Many real-world noise patterns such as radar clutter, radar jamming, and interference, atmospheric noise are non-Gaussian in nature. Many systems produce incorrect results in the presence of non-Gaussian noise [18,19,43,45]. Sigmoid-based fractional Fourier transform, sigmoid-based fractional Fourier ambiguity function, and sigmoid-based fractional Fourier Wigner–Ville distribution have been proposed to overcome the effect of impulse noise in parameter estimation of chirp signal. These sigmoid-based transforms do not require any prior knowledge of impulse noise [18,19]. Similar to sigmoid-based fractional Fourier-based ambiguity function and sigmoid-based fractional Fourier transform, a sigmoid-based GFAF and sigmoid-based GFWVD approach are proposed to reduce the effect of impulse noise on parameter estimation of higher-order chirps.

The remaining part of the paper is organized in the following manner. In Sect. 2, FrFT and GTFT are explained briefly along with some useful formulae. In Sect. 3, GFAF, GFWVD, and their properties are proposed. Section 4 presents the derivations

of the uncertainty principle for the GFAF and GFWVD. Section 5 presents the analysis of a multicomponent cubic chirp waveform and its parameter estimation using GFAF, along with its cross-term error analysis. In Sect. 6, the mathematical derivation and simulation results of multicomponent cubic chirps for SNR gain, mean square error (MSE), its comparison with other transforms are presented, and error propagation analysis has been performed. In Sect. 7, phase parameters of real multicomponent bat signal till fourth order of phase are estimated, and it is compared with the estimated parameter of FrFT-based AF. In Sect. 8, sigmoid GFAF and sigmoid GWVD are proposed for estimating higher-order chirp parameter in the presence of non-Gaussian noise. Finally, conclusions are drawn and future work is outlined.

2 Preliminaries

2.1 Different Time-Frequency Transforms

2.1.1 Fractional Fourier Transform

The fractional Fourier transform (FrFT) is a generalization of the Fourier transform (FT). It depends on the parameter α, which can be interpreted as an angle of rotation in the time-frequency (TF) plane [1,6,29,37,47,49]. The FrFT of a signal $x(t)$ is defined as

$$X_\alpha(f) = \int_{-\infty}^{+\infty} x(t) \cdot K_\alpha(t, f)\mathrm{d}t, \tag{1}$$

where the kernel $K_\alpha(t, f)$ of FrFT is given by [15]

$$K_\alpha(t, f) = \begin{cases} (\sqrt{1 - i\cot\alpha}) \cdot \exp\Big(i\pi t_0^2 f^2 \cot\alpha + i\pi f_0^2 t^2 \cot\alpha \\ \qquad\qquad -i2\pi f t \operatorname{cosec}\alpha\Big), & \text{if } \alpha \text{ is not a multiple of } \pi \\ \delta(f_0 t - t_0 f), & \text{if } \alpha \text{ is a multiple of } 2\pi \\ \delta(f_0 t + t_0 f), & \text{if } \alpha + \pi \text{ is a multiple of } 2\pi \end{cases}$$

where t_0, f_0 are dimensional normalization factors, $t_0^2 = \frac{T_{\max}}{f_s}$, $f_0^2 = \frac{f_s}{T_{\max}}$, $t_0^2 f_0^2 = 1$, $T_{\max}$ is the window length during FrFT and f_s is the sampling frequency. The unit of t_0 is second and f_0 is Hz.

It should be noted that at $\alpha = \frac{\pi}{2}$, K_α becomes the kernel of the Fourier transform, and hence, the FrFT of the signal becomes the Fourier transform of the signal. The FrFT is a linear transform, so it does not produce cross-terms during multicomponent signal analysis.

2.1.2 Generalized Time-Frequency Transform

If a signal $x(t)$ has a finite absolute sum (finite L^1 norm), then its generalized time-frequency transform (GTFT) evaluated at parameters (α, λ) is given by

$$X_{\alpha,\lambda}(f) = \int_{-\infty}^{+\infty} x(t) \cdot K_{\alpha,\lambda}(t, f)\mathrm{d}t, \tag{2}$$

where $K_{\alpha,\lambda}(t, f)$ is the kernel of GTFT and it is defined as [34–36]

$$K_{\alpha,\lambda}(t, f) = \begin{cases} \sqrt{1 - i\cot\alpha} \cdot \exp\Big(i\pi t_0^2 f^2 \cot\alpha + i\pi f_0^2 t^2 \cot\alpha \\ -i2\pi f t \operatorname{cosec}\alpha + i \cdot h(\lambda, t_0 f) - i \cdot h(\lambda, f_0 t)\Big), & \text{if } \alpha \text{ is not a multiple of } \pi \\ \delta(f_0 t - t_0 f), & \text{if } \alpha \text{ is a multiple of } 2\pi \\ \delta(f_0 t + t_0 f), & \text{if } \alpha + \pi \text{ is a multiple of } 2\pi \end{cases}$$

where $h(\cdot)$ is a real-valued dimensionless function, α, λ are the real-valued GTFT parameters and t_0, f_0 are dimensional normalization factors, $t_0^2 = \frac{T_{\max}}{f_s}$, $f_0^2 = \frac{f_s}{T_{\max}}$, $t_0^2 f_0^2 = 1$, $T_{\max}$ is the window length during GTFT and f_s is the sampling frequency. The unit of t_0 is second and unit of f_0 is Hz.

One speciality of the GTFT kernel is that it follows the property of index additivity of angle [36], i.e.,

$$\int_{-\infty}^{\infty} K_{\alpha_1,\lambda}(t, f) K_{\alpha_2,\lambda}(f, u)\mathrm{d}f = K_{(\alpha_1+\alpha_2),\lambda}(t, u). \tag{3}$$

The inverse GTFT is defined as [35]

$$x(t) = \int_{-\infty}^{\infty} X_{\alpha,\lambda}(f) \cdot K^*_{\alpha,\lambda}(t, f)\mathrm{d}f. \tag{4}$$

The GTFT can be used to analyze a much wider variety of frequency-modulated signals by varying $h(\cdot)$ in the GTFT kernel. Cubic-kernel-GTFT (ck-GTFT) is defined by substituting the parametric function $h(\cdot)$ as

$$h(\lambda, z) = \pi\lambda z^3. \tag{5}$$

It is to be noted that ck-GTFT is similar to the third-order polynomial Fourier transform (PFT) [14], with the added advantage of possessing the property of index additivity of angle.

Sinusoidal-kernel-GTFT is defined by substituting a multiparametric function $h(\cdot)$ as

$$h(A, \phi, \lambda, z) = A \sin(\pi\lambda z + \phi), \tag{6}$$

where A, ϕ, and λ are the variable parameters, which can be tuned to match the kernel with signal for estimating parameters. This can be a useful transform to analyze certain micro-Doppler effects in radar for the classification of rotating and vibrating targets [8,9].

2.2 Ambiguity Function and Its Variants

– **Ambiguity function**
For a given signal $x(t)$, the classical AF is defined as

$$A_x(\tau,\omega)=\int_{-\infty}^{\infty} x\left(t+\frac{\tau}{2}\right)x^*\left(t-\frac{\tau}{2}\right)\mathrm{e}^{-i\omega t}\mathrm{d}t. \tag{7}$$

If $X(\omega)$ is the FT of $x(t)$, then the AF is also defined as

$$A_X(v,\tau)=\int_{-\infty}^{\infty} X\left(\omega+\frac{v}{2}\right)X^*\left(\omega-\frac{v}{2}\right)\mathrm{e}^{i\omega\tau}\mathrm{d}\omega. \tag{8}$$

– **Wigner–Ville distribution**
For a given signal $x(t)$, the Wigner–Ville distribution (WVD) is defined as

$$W_x(t,\omega)=\int_{-\infty}^{\infty} x\left(t+\frac{\tau}{2}\right)x^*\left(t-\frac{\tau}{2}\right)\mathrm{e}^{-i\omega\tau}\mathrm{d}\tau. \tag{9}$$

– **Relation between AF and WVD**
The WVD can be expressed in terms of AF as

$$W_x(t,\omega)=\frac{1}{2\pi}\int_{-\infty}^{\infty}\int_{-\infty}^{\infty} A_x(\tau,v)\mathrm{e}^{-i(\omega\tau-vt)}dvd\tau. \tag{10}$$

– **Fractional Fourier transform or linear canonical transform-based ambiguity function**
Fractional Fourier transform or linear canonical transform (LCT)-based ambiguity function $\mathrm{AF}_x^A(\tau,f)$, of signal $x(t)$ is defined as [7,10,31,48]

$$\mathrm{AF}_x^A(\tau,f)=\int_{-\infty}^{\infty} x\left(t+\frac{\tau}{2}\right)y^*\left(t-\frac{\tau}{2}\right)K_\alpha(t,f)\mathrm{d}t. \tag{11}$$

Similarly, the WVD based on LCT $WVD_x^A(t,f)$ of signal $x(t)$ is defined as [33]

$$WVD_x^A(t,f)=\int_{-\infty}^{\infty} x\left(t+\frac{\tau}{2}\right)x^*\left(t-\frac{\tau}{2}\right)K_\alpha(t,f)\mathrm{d}\tau, \tag{12}$$

where $K_\alpha(t, f)$ is FrFT kernel and it is a special case of LCT kernel. LCT kernel is defined as follows:

$$K_A(t, f) = \frac{1}{\sqrt{i2\pi b}} \exp\left(i\frac{d}{2b}f^2 - i\frac{ft}{b} + i\frac{a}{2b}t^2\right).$$

2.3 Useful Formulae

2.3.1 Gaussian Integral

$$\int_{-\infty}^{+\infty} \mathrm{e}^{-At^2 \pm 2Bt + C}\,\mathrm{d}t = \sqrt{\frac{\pi}{A}}\mathrm{e}^{\frac{B^2}{A}+C}, \tag{13}$$

where $A, B, C \in \mathbb{C}$, $A \neq 0$, and $Re(A) \geq 0$ [47].

2.3.2 Principle of Stationary Phase

The principle of stationary phase (PSP) is used to obtain an approximate closed-form expression for the integral of a function whose amplitude $A(t)$ varies very slowly in comparison to the phase $\phi(t)$. Over the interval where the phase varies rapidly compared to amplitude, the contribution to the integral is negligible because positive and negative parts of the phase cancel each other. Hence, the nonzero contribution comes mainly from the stationary phase point 't_0' [42] which implies

$$\int_{-\infty}^{+\infty} A(t) \cdot \mathrm{e}^{i\phi(t)} \cdot \mathrm{d}t \approx \sqrt{\frac{2\pi}{\phi''(t_0)}} \cdot A(t_0)\mathrm{e}^{i\phi(t_0)} \cdot \mathrm{e}^{\frac{i\pi}{4}}, \tag{14}$$

where $\phi''(t)$ is second derivative of the phase function $\phi(t)$ and 't_0' is the point where derivative of the phase function becomes equal to 0 ($\phi'(t_0) = 0$). At this point, phase of the signal $\phi(t)$ is considered to be 'stationary.' If $t_0, t_1 \ldots t_n$ are the solutions of $\phi'(t) = 0$, then the integral can be approximated as

$$\int_{-\infty}^{+\infty} A(t) \cdot \mathrm{e}^{i\phi(t)} \cdot \mathrm{d}t \approx \sum_{k=0}^{n} \sqrt{\frac{2\pi}{\phi''(t_k)}} \cdot A(t_k)\mathrm{e}^{i\phi(t_k)} \cdot \mathrm{e}^{\frac{i\pi}{4}}. \tag{15}$$

This stationary phase approximation is accurate for high time-bandwidth products [11]. If a_0 is the coefficient of t in the phase function $\phi(t)$, then PSP is valid for $|a_0| >> 0$.

3 Proposed Definitions

3.1 Generalized Fractional Ambiguity Function and Generalized Fractional Wigner–Ville Distribution

All the above-stated algorithms can only estimate parameters of the chirp signals by compromising in computation complexity or parameter estimation accuracy and capable of analyzing only polynomial phase signals. However, in the synthetic aperture radar system during imaging of moving targets, ground-based radar, and sonar system, the reflected waveforms are required to be modeled as chirp signals with higher-order polynomial phase [2,4,14,17,30,42]. Therefore, a new kind of AF associated with GTFT called generalized fractional ambiguity function (GFAF) has been introduced.

For a given signal $x(t)$ with finite L^2 norm:

– The proposed GFAF associated with GTFT is defined as

$$\mathrm{AF}^{G}_{x(t),\alpha,\lambda}(\tau, f) = \int_{-\infty}^{\infty} x(t+\tau/2)x^{*}(t-\tau/2)K_{\alpha,\lambda}(t, f)\mathrm{d}t. \tag{16}$$

– The proposed generalized fractional Wigner–Ville distribution (GFWVD) associated with GTFT is defined as

$$WDF^{G}_{x(t),\alpha,\lambda}(t, f) = \int_{-\infty}^{\infty} x(t+\tau/2)x^{*}(t-\tau/2)K_{\alpha,\lambda}(\tau, f)\mathrm{d}\tau. \tag{17}$$

Here $K_{\alpha,\lambda}(t, f)$ is the kernel of GTFT. Cubic-kernel-GFAF (ck-GFAF) is defined as cubic-kernel-GTFT (ck-GTFT)-based ambiguity function. Similarly, cubic-kernel-GFWVD (ck-GFWVD) is defined as ck-GTFT-based WVD.

For two given signals $x(t)$ and $y(t)$ with finite L^2 norm:

– The proposed cross GFAF associated with GTFT is defined as

$$\mathrm{AF}^{G}_{x(t),y(t),\alpha,\lambda}(\tau, f) = \int_{-\infty}^{\infty} x(t+\tau/2)y^{*}(t-\tau/2)K_{\alpha,\lambda}(t, f)\mathrm{d}t. \tag{18}$$

– The proposed cross GFWVD associated with GTFT is defined as

$$WDF^{G}_{x(t),y(t),\alpha,\lambda}(t, f) = \int_{-\infty}^{\infty} x(t+\tau/2)y^{*}(t-\tau/2)K_{\alpha,\lambda}(\tau, f)\mathrm{d}\tau. \tag{19}$$

GFAF can perform waveform analysis and parameter estimation of a variety of signals (polynomial, sinusoidal frequency modulated, etc.) by appropriate selection of the parametric function $h(\cdot)$ in the GTFT kernel. For example, GFAF can use polynomial

phase GTFT kernel to analyze multicomponent polynomial phase signals. Cubic-kernel-GFAF (ck-GFAF) may be defined by using cubic-kernel GTFT to analyze multicomponent cubic frequency-modulated signals. On the other hand, GFAF can use sinusoidal-kernel GTFT to analyze multicomponent sinusoidal frequency-modulated phase signals. Furthermore, GFAF with the appropriately selected kernel can be used to analyze or estimate parameters of hybrid sinusoidal frequency-modulated polynomial phase signals. Similarly, parametric function $h(\cdot)$ of GTFT kernel can be appropriately selected for analyzing other types of signals.

3.2 Relation Between GFAF and GFWVD

From the definition of the GFAF and inverse transform property of GTFT, we have

$$x(t+\tau/2)x^*(t-\tau/2) = \int_{-\infty}^{\infty} \mathrm{AF}^G_{x(t),\alpha,\lambda}(\tau, f)K^*_{\alpha,\lambda}(t, f)\mathrm{d}f. \tag{20}$$

Hence, from the definition of GFWVD, we get

$$WDF^G_{x(t),\alpha,\lambda}(t, f') = \iint_{-\infty}^{\infty} \mathrm{AF}^G_{x(t),\alpha,\lambda}(\tau, f)K^*_{\alpha,\lambda}(t, f)K_{\alpha,\lambda}(\tau, f')\mathrm{d}\tau\mathrm{d}f, \tag{21}$$

where $K_{\alpha,\lambda}$ is the GTFT kernel.

3.3 Properties of Generalized Fractional Ambiguity Function

3.3.1 Relation with Other Ambiguity Functions

- If $h(\cdot) = 0$, then the GTFT kernel reduces to the fractional Fourier transform kernel, and therefore, the GFAF reduces to FrFT-based AF, and it is not linear.
- If $\alpha = 90°$, $h(\cdot) = 0$, then the GTFT kernel reduces to the Fourier transform kernel, and therefore, the GFAF reduces to classical AF, and it is not linear.

3.3.2 Inverse and Uniqueness Property of GFAF

If $x(t)$ has finite and nonzero L^2 norm, then there exists an a such that $x(a) \neq 0$. Additionally if the $\mathrm{AF}^G_{x(t),\alpha,\lambda}(\tau, f)$ has finite L^1 norm, we can define the unique inverse for GFAF as follows

$$x(t) = \frac{1}{x^*(a)} \int_{-\infty}^{\infty} \mathrm{AF}^G_{x(t),\alpha,\lambda}(t-a, f)K^*_{\alpha,\lambda}((t+a)/2, f)\mathrm{d}f. \tag{22}$$

Proof We know that

$$x(t+\tau/2)x^*(t-\tau/2) = \int_{-\infty}^{\infty} \mathrm{AF}^{G}_{x(t),\alpha,\lambda}(\tau, f) K^*_{\alpha,\lambda}(t, f)\mathrm{d}f. \tag{23}$$

Let $\tau/2 = t - a$, then Eq. (23) can be written as

$$x(2t-a)x^*(a) = \int_{-\infty}^{\infty} \mathrm{AF}^{G}_{x(t),\alpha,\lambda}(2(t-a), f) K^*_{\alpha,\lambda}(t, f)\mathrm{d}f. \tag{24}$$

Now, substitute $t = \frac{t+a}{2}$, thus we get

$$x(t) = \frac{1}{x^*(a)} \int_{-\infty}^{\infty} \mathrm{AF}^{G}_{x(t),\alpha,\lambda}(t-a, f) K^*_{\alpha,\lambda}\left(\frac{t+a}{2}, f\right)\mathrm{d}f. \tag{25}$$

Hence from Eq. (25), it is easy to see that for any nonzero $x(a)$, the inverse is unique for particular $x(t)$.

Also noteworthy is the case for $a = 0$, the form we obtain for the inverse in this case is

$$x(t) = \frac{1}{x^*(0)} \int_{-\infty}^{\infty} \mathrm{AF}^{G}_{x(t),\alpha,\lambda}(t, f) K^*_{\alpha,\lambda}(t/2, f)\mathrm{d}f. \tag{26}$$

□

3.3.3 Nonlinearity and Cross-terms

If multicomponent signal $z(t)$ is the sum of two monocomponent signals $x(t)$ and $y(t)$, respectively ($z(t) = x(t) + y(t)$), then GFAF of $z(t)$ can be expressed as:

$$\begin{aligned}\mathrm{AF}^{G}_{z(t),\alpha,\lambda}(\tau, f) = {} & \mathrm{AF}^{G}_{x(t),\alpha,\lambda}(\tau, f) + \mathrm{AF}^{G}_{y(t),\alpha,\lambda}(\tau, f) \\ & + \mathrm{AF}^{G}_{x(t),y(t),\alpha,\lambda}(\tau, f) + \mathrm{AF}^{G}_{y(t),x(t),\alpha,\lambda}(\tau, f).\end{aligned} \tag{27}$$

Here, as GFAF is a nonlinear transform, we can see that it produced cross-terms such as $\mathrm{AF}^{G}_{x(t),y(t),\alpha,\lambda}(\tau, f)$ and $\mathrm{AF}^{G}_{y(t),x(t),\alpha,\lambda}(\tau, f)$ during multicomponent signal analysis.

3.3.4 Total Energy Bound

Suppose that $x(t)$ has finite and nonzero L^2 norm, then we have

$$|\mathrm{AF}^{G}_{x(t),\alpha,\lambda}(\tau, f)| \leq |\sqrt{\mathrm{cosec}\alpha}| \int_{-\infty}^{\infty} |x(t)|^2 \mathrm{d}t. \tag{28}$$

So, the maximum value of GFAF is bounded by energy or L^2 norm of signal and fractional Fourier angle. This property can be proved using the Cauchy Schwarz inequality.

3.3.5 Total Energy Invariant Property

If $\alpha = 90^\circ$ and $\lambda = 0$, then GFAF gives the energy of signal $x(t)$ at origin, i.e.,

$$\mathrm{AF}^{G}_{x(t),\alpha=\frac{\pi}{2}\lambda=0,}(0, 0) = \int_{-\infty}^{\infty} |x(t)|^2 \mathrm{d}t. \tag{29}$$

3.3.6 Finite Time Delay Support Property

If $x(t)$ is zero for all t $\notin [t_1, t_2]$, then $\mathrm{AF}^{G}_{x(t),\alpha,\lambda}(\tau, f)$ is zero for all $\tau > t_2 - t_1$.

3.3.7 Symmetry and Conjugation Properties

The following properties can be proved:

Symmetry properties:

- $\mathrm{AF}^{G}_{x(t),\alpha,\lambda}(-\tau, f) = \left[\mathrm{AF}^{G}_{x(t),-\alpha,-\lambda}(\tau, f)\right]^*$, if $h(\lambda, \cdot)$ is an odd function of λ.
- $\mathrm{AF}^{G}_{x(t),\alpha,\lambda}(-\tau, -f) = \left[\mathrm{AF}^{G}_{x(t),-\alpha,-\lambda}(\tau, -f)\right]^*$, if $h(\lambda, \cdot)$ is an odd function of λ.

Conjugation Properties:

- $\mathrm{AF}^{G}_{x^*(t),\alpha,\lambda}(\tau, f) = \left[\mathrm{AF}^{G}_{x(t),-\alpha,-\lambda}(\tau, f)\right]^*$, if $h(\lambda, \cdot)$ is an odd function of λ.
- $\mathrm{AF}^{G}_{x(-t),\alpha,\lambda}(\tau, f) = \begin{cases} \mathrm{AF}^{G}_{x(t),\alpha,\lambda}(\tau, -f), & \text{if } h(\lambda, \cdot) \text{ is an even function of } t, f. \\ \mathrm{AF}^{G}_{x(t),\alpha,-\lambda}(\tau, -f), & \text{if } h(\cdot, \cdot \text{ is an odd function of } t, f \\ & \text{and } \lambda. \end{cases}$

$$-\mathrm{AF}^{G}_{x^*(-t),\alpha,\lambda}(\tau,f)=\begin{cases}\left[\mathrm{AF}^{G}_{x(t),-\alpha,-\lambda}(\tau,-f)\right]^*, & \text{if } h(\cdot,\cdot) \text{ is an even function of } t \\ & \text{and } f \text{ and an odd function of } \lambda. \\ \left[\mathrm{AF}^{G}_{x(t),-\alpha,\lambda}(\tau,-f)\right]^*, & \text{if } h(\cdot,\cdot) \text{ is an odd function of } t, \\ & f \text{ and } \lambda. \end{cases}$$

In particular, these properties are useful for ck-GFAF because for ck-GFAF, the GTFT kernel is an odd function of λ.

3.3.8 Time Delay Property

If ck-GFAF of $x(t)$ is $\mathrm{AF}^{G}_{x(t),\beta,\lambda}(\tau,f)$, then ck-GFAF of time delayed signal $x_1(t)=x(t-t_d)$ is given by

$$\mathrm{AF}^{G}_{x_1(t),\alpha,\lambda}(\tau,f)=C_0(f,\alpha,\lambda,t_d)\cdot\mathrm{AF}^{G}_{x(t),\beta,\lambda}(\tau,f'), \tag{30}$$

where

$$\cot\beta=\cot\alpha-3\lambda f_0 t_d,\quad f'=\frac{f\,\mathrm{cosec}\alpha-f_0^2 t_d\cot\alpha+\frac{3}{2}\lambda f_0^3 t_d^2}{\mathrm{cosec}\beta}\ \text{and}$$

$$C_0(f,\alpha,\lambda,t_d)=\frac{\sqrt{1-i\cot\alpha}}{\sqrt{1-i\cot\beta}}\cdot\exp\left(i\pi\left[-\lambda t_0^3 f'^3-t_0^2 f'^2\cot\beta+t_0^2 f^2\cot\alpha\right.\right.$$
$$\left.\left.+f_0^2 t_d^2\cot\alpha-2f t_d\mathrm{cosec}\alpha-\lambda f_0^3 t_d^3+\lambda t_0^3 f^3\right]\right).$$

If $\lambda=0$, then we can get a relationship equivalent to the time delay property of FrFT-based ambiguity function

$$\mathrm{AF}^{G}_{x_1(t),\alpha,\lambda=0}(\tau,f)=\mathrm{AF}^{G}_{x(t),\alpha}(\tau,f-f_0^2 t_d\cos\alpha) \tag{31}$$
$$\exp\left(i\pi\left[f_0^2 t_d^2\cos\alpha\sin\alpha-2f t_d\sin\alpha\right]\right), \tag{32}$$

where $\mathrm{AF}_{x(t),\alpha}$ is the ambiguity function in FrFT domain. Thus, a delay in time translates to the ambiguity function with a changed frequency.

3.3.9 Frequency Delay Property

If GFAF of $x(t)$ is $\mathrm{AF}^{G}_{x(t),\alpha,\lambda}(\tau,f)$, then GFAF of the frequency-modulated signal $x_1(t)=x(t)\mathrm{e}^{i\omega_d t}$ is given by

$$\mathrm{AF}^{G}_{x_1(t),\alpha,\lambda}(\tau,f)=\mathrm{e}^{i\omega_d\tau}\mathrm{AF}^{G}_{x(t),\alpha,\lambda}(\tau,f). \tag{33}$$

If $\lambda=0$ in Eq. (33), then we will get a relationship similar to that of a FrFT-based AF.

$$\mathrm{AF}^{G}_{x_1(t),\alpha,\lambda=0}(\tau,f)=\mathrm{AF}_{x(t),\alpha}(\tau,f)\mathrm{e}^{i\omega_d\tau},$$

where $\mathrm{AF}_{x(t),\alpha}$ is the ambiguity function in FrFT domain.

3.3.10 Time Scaling Property

If ck-GFAF of $x(t)$ is $\mathrm{AF}^{G}_{x(t),\beta,\lambda}(\tau, f)$, then ck-GFAF of $x_1(t) = \sqrt{a}x(at)$ is given by

$$AF^{G}_{x_1(t),\alpha,\lambda}(\tau, f) = C_0(f, \alpha, \lambda, a) \cdot \mathrm{AF}^{G}_{x(t),\beta,\lambda}\left(a\tau, \frac{f'}{a}\right), \tag{34}$$

where $\cot\beta = \frac{\cot\alpha}{a^2}$, $f' = \frac{f\,\mathrm{cosec}\alpha}{\mathrm{cosec}\beta}$, $\gamma_1 = \frac{\lambda}{a^3}$ and

$$C_0(f, \alpha, \lambda, a) = \frac{\sqrt{1 - i\cot\alpha}}{\sqrt{1 - i\cot\beta}} \cdot \exp\left(i\pi\left(\frac{\gamma_1 t_0^3 f'^3}{a^3}\left[a^6\left(\frac{\mathrm{cosec}\beta}{\mathrm{cosec}\alpha}\right)^3 - 1\right] + \left(\frac{t_0 f'}{a}\right)^2\left[a^2\left(\frac{\mathrm{cosec}\beta}{\mathrm{cosec}\alpha}\right)^2 \cdot \cot\alpha - \cot\beta\right]\right)\right).$$

If $\lambda = 0$ in Eq. (34), then we get a relationship like that of a FrFT-based ambiguity Function

$$\mathrm{AF}^{G}_{x_1(t),\alpha,\lambda=0}(\tau, f) = \frac{\sqrt{1 - i\cot\alpha}}{\sqrt{1 - i\cot\beta}} \cdot \exp\left(i\pi\left(\frac{t_0 f'}{a}\right)^2\left[a^2\left(\frac{\mathrm{cosec}\beta}{\mathrm{cosec}\alpha}\right)^2 \cot\alpha - \cot\beta\right]\right) \mathrm{AF}_{x(t),\beta}\left(a\tau, \frac{f'}{a}\right),$$

where $\mathrm{AF}_{x(t),\beta}(\tau, f')$ is fractional Fourier transform-based ambiguity function at angle β of signal $x(t)$.

3.3.11 Generalized Fractional Ambiguity Function in Terms of GTFT of Signal $x(t)$

If ck-GFAF of $x(t)$ is $\mathrm{AF}^{G}_{x(t),\alpha,\lambda}(\tau, f)$, then ck-GFAF in terms of GTFT is given by

$$\mathrm{AF}^{G}_{x(t),\alpha,\lambda}(\tau, f) = \frac{1}{\sqrt{1 - i\cot\beta}} \int_{-\infty}^{\infty} X_{\alpha,\lambda}(f_1) X^{*}_{\beta}(f') K^{*}_{\alpha,\lambda}(\tau, f_1) K_{\alpha,\lambda}(\tau/2, f) \cdot \mathrm{e}^{i\pi t_0^2 f'^2 \cot\beta} \mathrm{d}f_1, \tag{35}$$

where $\frac{3 f_0 \lambda \tau}{2} = -\cot\beta$ and $f' = \frac{-1}{\mathrm{cosec}\beta}\left[\frac{f_0^2 \tau}{2}\cot\alpha - f_1 \mathrm{cosec}\alpha + f\,\mathrm{cosec}\alpha - \frac{9\lambda f_0^3 \tau^2}{8}\right]$, and $X_\beta(f')$ is the FrFT of $x(t)$ at angle β.

If $\lambda = 0$ then $\beta = \frac{\pi}{2}$ so the GFAF becomes the ambiguity function in fractional Fourier domain.

$$\mathrm{AF}^{G}_{x(t),\alpha,\lambda=0}(\tau, f) = \int_{-\infty}^{\infty} X_{\alpha,\lambda=0}(f_1) X^{*}_{\frac{\pi}{2}}\left(-\frac{f_0^2 \tau}{2}\cot\alpha + f_1 \mathrm{cosec}\alpha - f\,\mathrm{cosec}\alpha\right) \cdot K^{*}_{\alpha,\lambda=0}(\tau, f_1) \cdot K_{\alpha,\lambda=0}(\tau/2, f) \mathrm{d}f_1.$$

3.3.12 Relationship of Generalized Fractional Ambiguity Function with STFrFT

If ck-GFAF of $x(t)$ is $\mathrm{AF}^{G}_{x(t),\alpha,\lambda}(\tau, f)$, then ck-GFAF is related to short time FrFT is given by

$$\mathrm{AF}^{G}_{x(t),\alpha,\lambda}(\tau, f) = C_0(\tau, f, \alpha, \lambda) \cdot X^{g}_{\beta}(\tau, f'),$$

where $X^{g}_{\beta}(\tau, f')$ is STFrFT at angle β with window function

$$g(t) = x(t) \cdot \exp(i\pi\lambda f_0^3 t^3),\ f' = \frac{1}{\mathrm{cosec}\beta} \cdot \left[f\mathrm{cosec}\alpha - \frac{9\lambda f_0^3 \tau^2}{8} + \frac{f_0^2 \tau \cot\alpha}{2} \right] \text{ and}$$

$$C_0(\tau, f, \alpha, \lambda) = \frac{\sqrt{1 - i\cot\alpha}}{\sqrt{1 - i\cot\beta}} \cdot \exp\left(i\pi \left[\frac{\tau^2 . f_0^2 \cot\alpha}{4} + t_0^2 f^2 \cot\alpha + f\tau\mathrm{cosec}\alpha \right.\right.$$
$$\left.\left. + \lambda t_0^3 f^3 - \frac{7\lambda f_0^3 \tau^3}{8} \right] \right).$$

If $\lambda = 0$, then we get the relation of fractional Fourier-based AF with short time Fourier transform (STFT).

$$\mathrm{AF}^{G}_{x(t),\alpha,\lambda=0}(\tau, f) = C_1(\tau, f, \alpha) \cdot X^{g_1}_{\frac{\pi}{2}}\left(\tau, -\frac{\tau f_0^2 \cot\alpha}{2} + f\mathrm{cosec}\alpha \right),$$

where $X^{g_1}_{\frac{\pi}{2}}\left(\tau, -\frac{\tau f_0^2 \cot\alpha}{2} + f\mathrm{cosec}\alpha \right)$ is STFT at angle $\pi/2$ with window function

$$g_1(t, \alpha) = x(t) \cdot \exp\left(-i\pi t^2 f_0^2 \cot\alpha \right),$$
$$C_1(\tau, f, \alpha) = \sqrt{1 - i\cot\alpha} \cdot \exp\left(i\pi \left[\frac{-3\tau^2 f_0^2 \cot\alpha}{4} + t_0^2 f^2 \cot\alpha + f\tau\mathrm{cosec}\alpha \right] \right).$$

3.3.13 Moyal Property

$$\int_{-\infty}^{\infty}\int \mathrm{AF}^{G}_{x(t),\alpha,\lambda}(\tau, f) \cdot \left[\mathrm{AF}^{G}_{y(t),\alpha,\lambda}(\tau, f) \right]^{*} \mathrm{d}\tau \mathrm{d}f = \left| \int_{-\infty}^{\infty} x(u) y^{*}(u) \mathrm{d}u \right|^2 \tag{36}$$

$$= |< x \cdot y >|^2, \tag{37}$$

where $< x \cdot y >$ is the standard inner product of the functions $x(\cdot)$ and $y(\cdot)$. GFAF follows total energy property and total energy of GFAF is equal to total energy of signal. Thus, the inner product of the two AFs can be found conveniently by using the value of inner product of the signals.

3.3.14 Multiplication Property

If signals $x(t)$ and $y(t)$ have respective ck-GFAFs $\mathrm{AF}^{G}_{x(t),\alpha,\lambda}(\tau, f_1)$ and $\mathrm{AF}^{G}_{y(t),\alpha,\lambda}(\tau, f_1)$, then a signal $z(t) = x(t) \cdot y(t)$ has an ck-GFAF $\mathrm{AF}^{G}_{z(t),\alpha,\lambda}(\tau, f)$ given by

$$\mathrm{AF}^{G}_{z(t),\alpha,\lambda}(\tau, f) = |\mathrm{cosec}\alpha| \int_{-\infty}^{\infty} \mathrm{AF}_{x(t),\alpha,\lambda}(\tau, f_1).\mathrm{AF}_{y(t),\frac{\pi}{2}}(\tau, (f - f_1)\mathrm{cosec}\alpha) \cdot \exp\left(i\pi\left[t_0^2 \cot\alpha(f^2 - f_1^2) + \lambda t_0^3(f^3 - f_1^3)\right]\right) \mathrm{d}f_1. \tag{38}$$

where $\mathrm{AF}_{y(t),\frac{\pi}{2}}(\tau, (f - f_1)\mathrm{cosec}\alpha) = \int_{-\infty}^{\infty} y(t + \frac{\tau}{2}) y^*(t - \frac{\tau}{2}) \mathrm{e}^{-i2\pi t \mathrm{cosec}\alpha(f - f_1)} \mathrm{d}t$, is Fourier transform-based ambiguity function. Thus, the ambiguity function of the multiplication of two signals, such as $z(t)$ can be computed in a convenient way by using the ambiguity functions of $x(t)$ and $y(t)$.

If $\lambda = 0$ and $\alpha = 90°$, Eq. (38) reduces to FFT-based ambiguity function

$$\mathrm{AF}^{G}_{z(t),\alpha=\frac{\pi}{2},\lambda=0}(\tau, f) = \mathrm{AF}_{x(t),\frac{\pi}{2}}(\tau, f) *_f \mathrm{AF}_{y(t),\frac{\pi}{2}}(\tau, f), \tag{39}$$

where $*_f$ is convolution over f.

3.3.15 Time Marginal Property

The time marginal property of the GFAF can be expressed by

$$\mathrm{AF}^{G}_{x(t),\alpha,\lambda}(0, f) = \int_{-\infty}^{\infty} |x(t)|^2 K_{\alpha,\lambda}(t, f) \mathrm{d}t. \tag{40}$$

3.3.16 Frequency Marginality Property

The frequency marginal property of the GFAF can be expressed by

$$\mathrm{AF}^{G}_{x(t),\alpha,\lambda}(\tau, 0) = \int_{-\infty}^{\infty} x(t + \tau/2) x^*(t - \tau/2) K_{\alpha,\lambda}(t, 0) \mathrm{d}t. \tag{41}$$

3.3.17 Cubic Phase Shift Property

The cubic kernel cross-generalized fractional ambiguity function of $x(t)$ and $y(t)$ is $\mathrm{AF}^{G}_{x(t),y(t),\alpha,\lambda}(\tau, f)$, and it is defined as follows:

$$\mathrm{AF}^{G}_{x(t),y(t),\alpha,\lambda}(\tau, f) = \int_{-\infty}^{\infty} x\left(t+\frac{\tau}{2}\right) y^{*}\left(t-\frac{\tau}{2}\right) K_{\alpha,\lambda}(t, f)\mathrm{d}t.$$

If $y(t) = x(t)\cdot \exp\left(i\pi[a_3t^3 + a_2t^2 + a_1t]\right)$, then assuming $a_3 = -f_0^3\lambda$ and $\frac{3a_3\tau}{2} + a_2 = f_0^2\cot\alpha$, $\mathrm{AF}^{G}_{x(t),y(t),\alpha,\lambda}(\tau, f)$ is given by

$$\mathrm{AF}^{G}_{x(t),y(t),\alpha,\lambda}(\tau, f) = c_0(\tau, f, \alpha, \lambda)\cdot \mathrm{AF}_{x(t),\frac{\pi}{2}}\left(\tau, f\operatorname{cosec}\alpha + \frac{a_1}{2} + \frac{3\tau^2 a_3}{8} - \frac{a_2\tau}{2}\right), \tag{42}$$

where $\mathrm{AF}_{x(t),\frac{\pi}{2}}(\tau, f)$ is the Fourier transform-based ambiguity function and $c_0(\tau, f, \alpha, \lambda) = \sqrt{1 - i\cot\alpha}\cdot\exp\left(i\pi\left[\frac{-a_3\tau^3}{8} - \frac{a_2\tau^2}{4} + \frac{a_1\tau}{2} + \lambda t_0^3 f^3 + t_0^2 f^2\cot\alpha\right]\right)$.

3.3.18 Property of Index Additivity of Angle for GFAF

Since GFAF follows the property of index additivity of angle, it is computationally efficient, i.e.,

$$\mathrm{AF}^{G}_{x(t),\alpha+\beta,\lambda}(\tau, u) = \int_{-\infty}^{+\infty} \mathrm{AF}^{G}_{x(t),\alpha,\lambda}(\tau, f) K_{\beta,\lambda}(f, u)\mathrm{d}f. \tag{43}$$

3.3.19 Computational Complexity of Digital GFAF

GFAF is the GTFT of the autocorrelation of a signal. The computational requirement of the GTFT for an N length quadratic chirp signal is $O(N\log_2 N)$. With the correlation of the signal added, the digital computational complexity of GFAF becomes $O(N^2\log_2 N)$ [5,12,16,40]. Comparison of the computational complexity of different higher-order transform are shown in Table 1. As shown in Table 1, the computational complexity of GFAF is lesser than generalized cubic phase function (GCPF), maximum likelihood (ML), and QML estimator for estimating higher-order chirp parameters.

Table 1 Comparison of computational complexity of different higher-order transform

Higher-order transform	GFAF	ML	HAF	GCPF	Hybrid CPF-HAF	QML
Computational complexity	$O(N^2 \log_2 N)$	$O(N^{P+1})$	$O(PN \log_2 N)$	$O(N^3)$	$O(N^2)$	$O(N^3)$

4 Uncertainty Principle for GFAF

Consider a unit energy signal $x(t)$ and its GTFT as $X_{\alpha,\lambda}(\cdot)$. Let τ_{mean} be mean time and f_{mean} be mean frequency of $x(t)$.

$$\int_{-\infty}^{\infty} |x(\tau)|^2 \mathrm{d}\tau = 1 \text{ and } \int_{-\infty}^{\infty} |X_{\alpha,\lambda}(f)|^2 \mathrm{d}f = 1,$$
$$\int_{-\infty}^{\infty} \tau |x(\tau)|^2 \mathrm{d}\tau = \tau_{\text{mean}} \text{ and } \int_{-\infty}^{\infty} f |X_{\alpha,\lambda}(f)|^2 \mathrm{d}f = f_{\text{mean}}.$$

Now, consider time variance of GFAF is $\sigma^2_{t_{GFAF}}$ given by:

$$\begin{aligned}
\sigma^2_{\text{tGFAF}} &= \iint_{-\infty}^{\infty} (\tau - \tau_{\text{mean}})^2 |\text{AF}^G_{x(t),\alpha,\lambda}(\tau, f)|^2 \mathrm{d}\tau \mathrm{d}f, \\
&= \int_{-\infty}^{\infty} (\tau - \tau_{\text{mean}})^2 \int_{-\infty}^{\infty} \int_{-\infty}^{\infty} x(t + \tau/2) x^*(t - \tau/2) \\
&\quad x^*(t' + \tau/2) x(t' - \tau/2). \left[\int_{-\infty}^{\infty} K_{\alpha,\lambda}(t, f)^* K_{\alpha,\lambda}(t', f) \mathrm{d}f \right] \mathrm{d}t \mathrm{d}t' \mathrm{d}\tau, \\
&= \iint_{-\infty}^{\infty} (\tau - \tau_{\text{mean}})^2 |x(t + \tau/2)|^2 |x(t - \tau/2)|^2 \mathrm{d}\tau \mathrm{d}t. \qquad (44)
\end{aligned}$$

Put $t + \tau/2 = m$, and $t - \tau/2 = n$. If $x(t)$ is real and zero mean, then $\tau_{\text{mean}} = 0$. Hence, the time-variance is given by:

$$\sigma^2_{\text{tGFAF}} = \iint_{-\infty}^{\infty} (m - n)^2 |x(m)|^2 |x(n)|^2 \mathrm{d}m \mathrm{d}n = 2 \int_{-\infty}^{\infty} m^2 |x(m)|^2 \mathrm{d}m. \qquad (45)$$

Now consider frequency variance of GFAF is $\sigma^2_{\mathrm{f_{GFAF}}}$

$$\begin{aligned}\sigma^2_{\mathrm{f_{GFAF}}} &= \iint_{-\infty}^{\infty} (f - f_{\mathrm{mean}})^2 |\mathrm{AF}^G_{X_{\alpha,\lambda}(u),\alpha,\lambda}(f,\tau)|^2 \mathrm{d}\tau \mathrm{d}f \\ &= \int_{-\infty}^{\infty} (f - f_{\mathrm{mean}})^2 \int_{-\infty}^{\infty} X_{\alpha,\lambda}(u + f/2) X^*_{\alpha,\lambda}(u - f/2) \int_{-\infty}^{\infty} X^*_{\alpha,\lambda}(u' + f/2) \\ &\quad X_{\alpha,\lambda}(u' - f/2). \left[\int_{-\infty}^{\infty} K_{\alpha,\lambda}(u,\tau)^* K_{\alpha,\lambda}(u',\tau) \mathrm{d}\tau \right] \mathrm{d}u \mathrm{d}u' \mathrm{d}f \\ &= \iint_{-\infty}^{\infty} (f - f_{\mathrm{mean}})^2 |X_{\alpha,\lambda}(u + f/2)|^2 |X_{\alpha,\lambda}(u - f/2)|^2 \mathrm{d}u \mathrm{d}f. \end{aligned} \tag{46}$$

Put $u + f/2 = w$, and $u - f/2 = v$, If $x(t)$ is real and zero mean, then $f_{\mathrm{mean}} = 0$. Hence, the frequency-variance is given

$$\sigma^2_{f_{GFAF}} = \iint_{-\infty}^{\infty} (w - v)^2 |X_{\alpha,\lambda}(w)|^2 |X_{\alpha,\lambda}(v)|^2 \mathrm{d}w \mathrm{d}v = 2 \int_{-\infty}^{\infty} w^2 |X_{\alpha,\lambda}(w)|^2 \mathrm{d}w. \tag{47}$$

From Eqs. (45) and (47), square of time bandwidth product (TBP) can be written as:

$$\sigma^2_{\mathrm{t_{GFAF}}} \sigma^2_{\mathrm{f_{GFAF}}} = 4 \int_{-\infty}^{\infty} m^2 |x(m)|^2 \mathrm{d}m \int_{-\infty}^{\infty} w^2 |X_{\alpha,\lambda}(w)|^2 \mathrm{d}w = 4 \cdot \sigma^2_{\mathrm{t_{GTFT}}} \sigma^2_{\mathrm{f_{GTFT}}},$$

where $\sigma^2_{\mathrm{t_{GTFT}}}$ is time variance and $\sigma^2_{\mathrm{f_{GTFT}}}$ is frequency variance of GFAF, and their product is always greater than or equal to $\sin^2 \alpha/4$ [36], i.e.,

$$\begin{aligned} \sigma^2_{\mathrm{t_{GFAF}}} \cdot \sigma^2_{\mathrm{f_{GFAF}}} &\geq 4 \cdot \frac{\sin^2 \alpha}{4} \\ \therefore \sigma_{\mathrm{t_{GFAF}}} \cdot \sigma_{\mathrm{f_{GFAF}}} &\geq |\sin \alpha|. \end{aligned} \tag{48}$$

Similarly, we can also derive the uncertainty principle or TBP for generalized fractional Wigner–Ville distribution:

$$\sigma_{\mathrm{t_{GFWVD}}} \cdot \sigma_{\mathrm{f_{GFWVD}}} \geq \frac{|\sin \alpha|}{4}, \tag{49}$$

where $\sigma^2_{\mathrm{t_{GFWVD}}}$ is time variance and $\sigma^2_{\mathrm{f_{GFWVD}}}$ is frequency variance of GFWVD.

5 Pulsed Cubic Chirp Waveform Analysis Using ck-GFAF

5.1 Mathematical Derivation of Pulsed Cubic Chirp Waveform Analysis Using ck-GFAF

5.1.1 Unmatched Case

Consider a signal

$$x(t) = A \cdot \mathrm{rect}\left(\frac{t}{T}\right) \cdot \exp\left[i\pi\left(a_1 t + a_2 t^2 + a_3 t^3 + a_4 t^4\right)\right], \tag{50}$$

where

$$\mathrm{rect}\left(\frac{t}{T}\right) = \begin{cases} 1, & -\frac{T}{2} \le t \le \frac{T}{2}, \\ 0, & \text{otherwise.} \end{cases}$$

Then its instantaneous correlation becomes

$$x(t+\tau/2)x^*(t-\tau/2) = |A|^2 \cdot \mathrm{rect}\left(\frac{t}{T-|\tau|}\right) \cdot \exp\left[i\pi\left(4a_4\tau t^3 + 3a_3\tau t^2 + (2a_2\tau + a_4\tau^3)t + a_1\tau + \frac{a_3\tau^3}{4}\right)\right].$$

Consider the ck-GTFT kernel given by Eq. (5) with $h(\lambda, t_0 f) = i\pi\lambda(t_0 f)^3$ and $h(\lambda, f_0 t) = i\pi\lambda(f_0 t)^3$ to be

$$K_{\alpha,\lambda}(t, f) = \sqrt{1 - i.\mathrm{cot}\alpha} \cdot \exp\left[i\pi\left(t_0^2 f^2 \mathrm{cot}\alpha + f_0^2 t^2 \mathrm{cot}\alpha - 2ft\,\mathrm{cosec}\alpha + \lambda(t_0 f)^3 - \lambda(f_0 t)^3\right)\right]. \tag{51}$$

Then, by the applying the PSP approximation, GFAF of the signal $x(t)$ becomes

$$\left|\mathrm{AF}^G_{x(t),\alpha,\lambda}(\tau, f)\right| \approx \left| \sqrt{\frac{|A|^2 \mathrm{cosec}\alpha}{\sqrt{\left(3a_3\tau + f_0^2\mathrm{cot}\alpha\right)^2 - 6\left(4a_4\tau - f_0^3\lambda\right)\left(a_2\tau + \frac{a_4\tau^3}{2} - f\,\mathrm{cosec}\alpha\right)}}} \cdot \left(e^{i\phi_{20}} \cdot \mathrm{rect}\left(\frac{t_1}{T-|\tau|}\right) + i e^{-i\phi_{20}} \cdot \mathrm{rect}\left(\frac{t_2}{T-|\tau|}\right)\right)\right|,$$

where

$$t_{1,2} = \underbrace{\frac{-a'}{3c'}}_{\alpha_0} \pm \underbrace{\frac{\sqrt{a'^2 - 6c'f'}}{3c'}}_{\beta_0},$$

$$\phi_{20} = \pi\left[c'(\beta_0^3 + 3\beta_0\alpha_0^2) + 2a'\alpha_0\beta_0 + 2f'\beta_0\right],$$
$$\alpha_0 = \frac{-a'}{3c'}, \beta_0 = \frac{\sqrt{a'^2 - 6c'f'}}{3c'},\ c' = 4a_4\tau - f_0^3\lambda,$$
$$a' = 3a_3\tau + f_0^2\cot\alpha,\ f' = a_2\tau + \frac{a_4\tau^3}{2} - f\operatorname{cosec}\alpha. \tag{52}$$

5.1.2 Cubic Phase-Matched Case

If $4a_4\tau = f_0^3\lambda$ and $3a_3\tau \neq -f_0^2\cot\alpha$, then

$$\mathrm{AF}^G_{x(t),\alpha,\lambda}(\tau, f) = |A|^2\sqrt{1 - i\cot\alpha}\int_{-\infty}^{\infty}\operatorname{rect}\left(\frac{t}{T-|\tau|}\right)\cdot\exp\left[i\pi\left((3a_3\tau + f_0^2\cot\alpha)t^2 + (2a_2\tau + a_4\tau^3 - 2f\operatorname{cosec}\alpha)t + t_0^2f^2\cot\alpha + \lambda(t_0f)^3 + a_1\tau + \frac{a_3\tau^3}{4}\right)\right]\mathrm{d}t.$$

Let $C_0(\tau, f, \alpha) = 2a_2\tau + a_4\tau^3 - 2f\operatorname{cosec}\alpha$ and $C_1(\tau, \alpha) = 3a_3\tau + f_0^2\cot\alpha$, then we get:

$$\left|\mathrm{AF}^G_{x(t),\alpha,\lambda}(\tau, f)\right| = |A|^2\sqrt{\operatorname{cosec}\alpha}\left|\int_{-\infty}^{\infty}\operatorname{rect}\left(\frac{t}{T-|\tau|}\right)\cdot\exp\left[i\pi\left(C_1t^2 + C_0t\right)\right]\mathrm{d}t\right|.$$

Applying PSP approximation,

$$\left|\mathrm{AF}^G_{x(t),\alpha,\lambda}(\tau, f)\right| \approx |A|^2\sqrt{\frac{\operatorname{cosec}\alpha}{C_1}},\qquad -\frac{T-|\tau|}{2} \leq -\frac{C_0}{2C_1} \leq \frac{T-|\tau|}{2}. \tag{53}$$

5.1.3 Cubic and Quadratic Phase-Matched Case

If $4a_4\tau = f_0^3\lambda$, $3a_3\tau = -f_0^2\cot\alpha$ and $2a_2\tau + a_4\tau^3 \neq 2f\operatorname{cosec}\alpha$, then

$$\mathrm{AF}^G_{x(t),\alpha,\lambda}(\tau, f) = |A|^2\sqrt{1 - i\cot\alpha}\int_{-\infty}^{\infty}\operatorname{rect}\left(\frac{t}{T-|\tau|}\right)\exp\left[i\pi\left(t_0^2f^2\cot\alpha + \lambda(t_0f)^3 + (2a_2\tau + a_4\tau^3 - 2f\operatorname{cosec}\alpha)t + a_1\tau + \frac{a_3\tau^3}{4}\right)\right]\mathrm{d}t.$$

$$\left|\mathrm{AF}^G_{x(t),\alpha,\lambda}(\tau, f)\right| = |A|^2\sqrt{\operatorname{cosec}\alpha}\int_{-\frac{T-|\tau|}{2}}^{\frac{T-|\tau|}{2}}\exp[i\pi(2a_2\tau + a_4\tau^3 - 2f\operatorname{cosec}\alpha)t]\mathrm{d}t.$$

$$\left|\mathrm{AF}^G_{x(t),\alpha,\lambda}(\tau, f)\right| = |A|^2\sqrt{\operatorname{cosec}\alpha}\cdot\frac{\exp\left[\frac{i\pi C_0(T-|\tau|)}{2}\right] - \exp\left[-\frac{i\pi C_0(T-|\tau|)}{2}\right]}{i\pi C_0},$$

where $C_0(\tau, f, \alpha) = 2a_2\tau + a_4\tau^3 - 2f\,\mathrm{cosec}\alpha$.

$$\left|\mathrm{AF}^G_{x(t),\alpha,\lambda}(\tau, f)\right| = 2|A|^2\sqrt{\mathrm{cosec}\alpha}\cdot\frac{\sin\left[\frac{\pi C_0(T-|\tau|)}{2}\right]}{\pi C_0}, \tag{54}$$

$$\left|\mathrm{AF}^G_{x(t),\alpha,\lambda}(\tau, f)\right| = 2|A|^2\sqrt{\mathrm{cosec}\alpha}\cdot\frac{\sin\left[\frac{\pi(2a_2\tau+a_4\tau^3-2f\,\mathrm{cosec}\alpha)(T-|\tau|)}{2}\right]}{\pi(2a_2\tau + a_4\tau^3 - 2f\,\mathrm{cosec}\alpha)}, \quad -T \le \tau \le T. \tag{55}$$

From Eq. (55), the zero-Doppler response can be given by

$$\left|\mathrm{AF}^G_{x(t),\alpha,\lambda}(\tau, 0)\right| = 2|A|^2\sqrt{\mathrm{cosec}\alpha}\cdot\frac{\sin\left[\frac{\pi(2a_2\tau+a_4\tau^3)(T-|\tau|)}{2}\right]}{\pi(2a_2\tau + a_4\tau^3)}, \quad -T \le \tau \le T. \tag{56}$$

With the zero-range and zero-Doppler responses, we can find range and Doppler resolutions as follows:

From Eq. (56), the first zero occurs when

$$T = |\tau| + \frac{2}{2a_2\tau + a_4\tau^3}. \tag{57}$$

Hence, range resolution $\Delta R = c\tau_0/2$, where τ_0 is the smallest positive root of Eq. (57) and 'c' is the velocity of light.

From Eq. (55), the zero-delay response is given by

$$\left|\mathrm{AF}^G_{x(t),\alpha,\lambda}(0, f)\right| = |A|^2\sqrt{\mathrm{cosec}\alpha}\cdot\frac{\sin[\pi T f\,\mathrm{cosec}\alpha]}{\pi f\,\mathrm{cosec}\alpha}. \tag{58}$$

5.1.4 Waveform Analysis Using Different GFAFs

Multicomponent chirp signal $x(t) = x_1(t) + x_2(t)$ is considered, where

$$x_1(t) = \mathrm{e}^{i\pi\left(a_1t+a_2t^2+a_3t^3+a_4t^4\right)}, \quad -2 \le t < 2 \text{ (in seconds)} \tag{59}$$

$$x_2(t) = \mathrm{e}^{i\pi\left(b_1t+b_2t^2+b_3t^3+b_4t^4\right)}, \quad -2 \le t < 2 \text{ (in seconds)} \tag{60}$$

are two fourth-order chirp signals.

Simulations have been done to analyze multicomponent cubic chirp signals, and the respective AF plots are obtained by focusing at each individual component and also focusing at both the components. The parameters used for the above simulation are $a_1 = 4$, $a_2 = 4$, $a_3 = 4$, $a_4 = 4$, $\lambda_a = 18.7880$ and $\alpha_a = 0.8087$ for the first component and $b_1 = 20$, $b_2 = 15$, $b_3 = 10$, $b_4 = 5$, $\lambda_b = 20$ and $\alpha_b = -1$ for the second component. Here, α_a, λ_a and α_b, λ_b are the matched ck-GTFT kernel parameters for first and second components, respectively. We consider $f_s = 200\ Hz$ as the sampling frequency. At the matched condition, the GFAF should produce an impulse, which can be seen in Figs. 1 and 2.

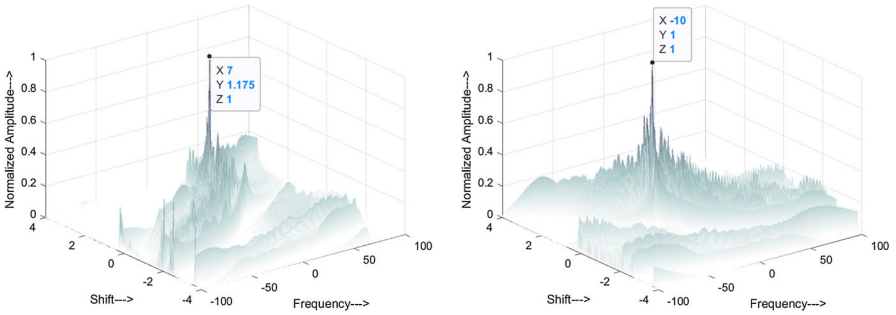

(a) First Component **(b)** Second Component

Fig. 1 The cubic kernel GTFT-based GFAF plot for multicomponent cubic chirp signal focused at individual components

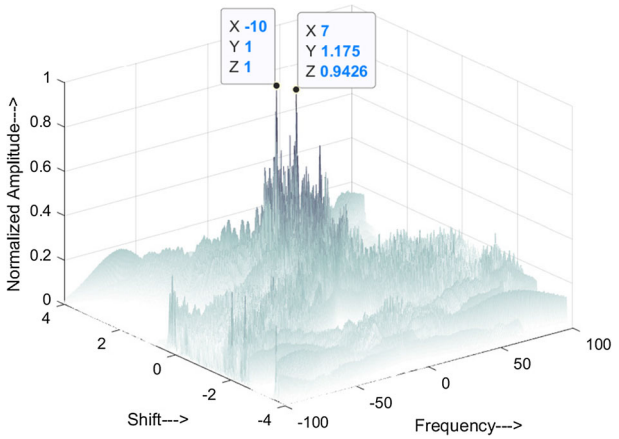

Fig. 2 The cubic kernel GTFT-based GFAF plot for multicomponent cubic chirp signal

5.2 Extraction of Fourth-Order Chirp Parameters Using ck-GFAF

5.2.1 Proposed Method

Consider a signal $x(t) = A_0 \cdot \exp\left(i\pi\left[a_1 t + a_2 t^2 + a_3 t^3 + a_4 t^4\right]\right)$. Now its instantaneous correlation is

$$x(t)x^*(t-\tau) = |A_0|^2 \cdot \exp\left(i\pi\left[4a_4\tau t^3 + (3a_3\tau - 6a_4\tau^2)t^2 + (2a_2\tau - 3a_3\tau^2 + a_4\tau^3)t\right]\right).$$

Now considering ck-GTFT, the kernel then becomes

$$K_{\alpha,\lambda}(t, f) = (\sqrt{1 - i\cot\alpha}) \cdot \exp\Big(i\pi t_0^2 f^2 \cot\alpha + i\pi f_0^2 t^2 \cot\alpha - i \cdot 2\pi f t \operatorname{cosec}\alpha + i\pi\lambda t_0^3 f^3 - i\pi\lambda f_0^3 t^3\Big). \quad (61)$$

Now, if the GFAF has to show an impulse in the delay-Doppler domain, two conditions have to be satisfied so that the cubic and quadratic phase coefficients will be matched to the cubic and quadratic phase coefficients of GTFT kernel.

$$4a_4\tau = f_0^3\lambda. \tag{62}$$

$$3a_3\tau - 6a_4\tau^2 = -f_0^2\cot\alpha, \tag{63}$$

The location on frequency axis of the impulse is given by the following equation

$$2a_2\tau - 3a_3\tau^2 + 4a_4\tau^3 = 2f\operatorname{cosec}\alpha. \tag{64}$$

The method used for estimating the parameters of a single as well as multicomponent chirp signal is as follows:

1. Iterate τ over the range $(-T_{\max}, T_{\max})$, where $T_{\max}$ is the length of the signal. Initially, rough estimation of chirp parameters can be obtained for reducing the search range of parameters using STFT estimation. STFT cannot provide excellent parameter estimation due to the dispersive nature of cubic chirp in the Fourier domain. Fine parameter search for the entire range of τ is done, as explained in further steps.
   (a) For each τ in the range, we obtain a range for α and λ using Eqs. (62–64). Perform fine search for $\alpha \in (\alpha_{\min}, \alpha_{\max})$, $\lambda \in (\lambda_{\min}, \lambda_{\max})$, and find optimum $\hat{\alpha}_{\text{opt}}$ and optimum $\hat{\lambda}_{\text{opt}}$ which gives the maximum peak amplitude of GFAF, per value of τ.
   (b) Estimate parameters a_4^{est}, a_3^{est} and a_2^{est} using optimum $\hat{\alpha}_{\text{opt}}$ and optimum $\hat{\lambda}_{\text{opt}}$.
   (c) Multiply the signal with $e^{-i\pi(\hat{a_4}^{\text{est}}t^4+\hat{a_3}^{\text{est}}t^3+\hat{a_2}^{\text{est}}t^2)}$ which reduces the signal to be of the form $e^{i\pi(a_1t+err)}$, where err is the error in conjugate multiplication as a result of errors in estimating a_4, a_3 and a_2.
   (d) Find the maximum amplitude (say A_τ) of the Fourier transform of the resultant signal.
2. Repeat step 1 (a-d) for all τ.
3. Now, take the τ value which gives the maximum of all A_τ values as τ_{opt} and the corresponding $\hat{\alpha}_{\text{opt}}$, $\hat{\lambda}_{\text{opt}}$ as $\alpha_{\text{opt}}^{\text{est}}$, $\lambda_{\text{opt}}^{\text{est}}$.
4. Finally, the chirp parameters a_4^{est}, a_3^{est},a_2^{est} and a_1^{est} are estimated using $\alpha_{\text{opt}}^{\text{est}}$, $\lambda_{\text{opt}}^{\text{est}}$.

5.2.2 Cross-terms Analysis for Multicomponent Chirps

Suppose we have a multicomponent signal $x(t)$ given by

$$x(t) = x_1(t) + x_2(t), \tag{65}$$

where $x_1(t)$ and $x_2(t)$ are single component cubic chirp signals:

$$\begin{aligned} x_1(t) &= A_0\exp(i\pi(a_1t + a_2t^2 + a_3t^3 + a_4t^4)), \\ x_2(t) &= A_0\exp(i\pi(b_1t + b_2t^2 + b_3t^3 + b_4t^4)). \end{aligned} \tag{66}$$

Then the correlation is given by

$$x(t)x^*(t-\tau)=\underbrace{x_1(t)x_1^*(t-\tau)+x_2(t)x_2^*(t-\tau)}_{\text{autoterms}}+\underbrace{x_1(t)x_2^*(t-\tau)+x_2(t)x_1^*(t-\tau)}_{\text{cross-terms}}.$$

We have the ambiguity functions for the auto-terms given as follows:

$$\begin{aligned}\underbrace{\mathrm{AF}_{(x_1,x_1^*)}(\tau,f)}_{\text{auto-term1}} &= \int_{-\infty}^{\infty}|A_0|^2\cdot\exp[i\pi(4a_4\tau t^3+(3a_3\tau-6a_4\tau^2)t^2\\ &\quad+(2a_2\tau-3a_3\tau^2+a_4\tau^3)t)]\cdot K_{\alpha,\lambda}(t,f)\mathrm{d}t,\\ \underbrace{\mathrm{AF}_{(x_2,x_2^*)}(\tau,f)}_{\text{auto-term2}} &= \int_{-\infty}^{\infty}|A_0|^2\cdot\exp[i\pi(4b_4\tau t^3+(3b_3\tau-6b_4\tau^2)t^2\\ &\quad+(2b_2\tau-3b_3\tau^2+b_4\tau^3)t)]\cdot K_{\alpha,\lambda}(t,f)\mathrm{d}t.\end{aligned}$$

The matched condition for auto-term 1 is given by:

$$\begin{aligned}4a_4\tau &= f_0^3\lambda_{\mathrm{opt}_1},\\ 3a_3\tau-6a_4\tau^2 &= -f_0^2\cot\alpha_{\mathrm{opt}_1},\end{aligned}\tag{67}$$

where α_{opt_1} and λ_{opt_1} are optimum α and optimum λ corresponding to first auto-term. The location of the impulse for auto-term 1 in GFAF domain is given by:

$$f_{\mathrm{peak}_1}=[2a_2\tau-3a_3\tau^2-a_4\tau^3]\sin\alpha_{\mathrm{opt}_1}.\tag{68}$$

Similarly the matched condition for auto-term 2 is given by:

$$\begin{aligned}4b_4\tau &= f_0^3\lambda_{\mathrm{opt}_2},\\ 3b_3\tau-6b_4\tau^2 &= -f_0^2\cot\alpha_{\mathrm{opt}_2},\end{aligned}\tag{69}$$

where α_{opt_2} and λ_2 are optimum α and optimum λ corresponding to second auto-term. The location of the impulse for auto-term 2 in GFAF domain is given by:

$$f_{\mathrm{peak}_2}=[2b_2\tau-3b_3\tau^2-b_4\tau^3]\sin\alpha_{\mathrm{opt}_2}.\tag{70}$$

Now looking at cross-term 1, we have

$$\begin{aligned}\mathrm{AF}^G_{(x_1,x_2^*)}(\tau,f) &= \int_{-\infty}^{\infty}|A_0|^2\cdot\exp[i\pi((a_4-b_4)t^4+(a_3-b_3+4b_4\tau-\lambda f_0^3)t^3\\ &\quad+(a_2-b_2+3\tau b_3-6b_4\tau^2+f_0^2\cot\alpha)t^2+(a_1-b_1-3b_3\tau^2\\ &\quad+4b_4\tau^3+2b_2\tau-2f\operatorname{cosec}\alpha)t)]\mathrm{d}t.\end{aligned}\tag{71}$$

From Eq. (71), we see that when $a_4 \neq b_4$, the amplitude of the cross-terms will be lesser than the impulse generated by the auto-terms. This is because no impulse can be produced by the cross-terms when $a_4 \neq b_4$. However, when $a_4 = b_4$, cross-terms can produce impulse and give false information regarding auto-terms.

Now consider the case of $a_4 = b_4$. The matched condition for the above cross-term 1 to be an impulse is

$$\begin{aligned} a_3 - b_3 &= f_0^3\lambda - 4b_4\tau, \\ a_2 - b_2 &= -f_0^2\cot\alpha - 3b_3\tau + 6b_4\tau^2, \end{aligned} \tag{72}$$

with the peak produced in GFAF domain at

$$2f = [a_1 - b_1 - 3b_3\tau^2 + 4b_4\tau^3 + 2b_2\tau]\sin\alpha. \tag{73}$$

τ varies from $[-T, T]$. Using matched condition given in Eqs. (69) and (67), we get the range of $a_3 - b_3$ and $a_2 - b_2$ as

$$\begin{aligned} &-8b_4T < a_3 - b_3 < 8b_4T, \\ &\min(6b_3T, 3(a_3 + b_3)T) - 12b_4T^2 < a_2 - b_2 < \max(-6b_3T, -3(a_3 + b_3)T) \\ &+ 12b_4T^2. \end{aligned} \tag{74}$$

The same analysis can be performed for cross-term 2 as well. We then get

$$\begin{aligned} b_3 - a_3 &= f_0^3\lambda - 4a_4\tau, \\ b_2 - a_2 &= -f_0^2\cot\alpha - 3a_3\tau + 6a_4\tau^2. \end{aligned} \tag{75}$$

with the peak produced in GFAF domain at

$$2f = [b_1 - a_1 - 3a_3\tau^2 + 4a_4\tau^3 + 2a_2\tau]\sin\alpha. \tag{76}$$

τ varies from $[-T, T]$. Using matched condition given in Eqs. (69) and (67), we get the range of $a_3 - b_3$ and $a_2 - b_2$ as

$$\begin{aligned} &-8a_4T < a_3 - b_3 < 8a_4T, \\ &\min(6a_3T, 3(a_3 + b_3)T) - 12a_4T^2 < a_2 - b_2 < \max(-6a_3T, -3(a_3 + b_3)T) \\ &+ 12a_4T^2. \end{aligned} \tag{77}$$

We can reduce our search range by roughly estimating a_1^{est}, a_2^{est}, a_3^{est}, and a_4^{est} using STFT or PFT. Therefore, using conditions for both cross-term 1 and cross-term 2 to not produce impulse, we need either of the following conditions:

$$
\begin{aligned}
& a_4 \neq b_4, \\
& |b_3 - a_3| > \max(8a_4^{\text{est}}T, 8b_4^{\text{est}}T), \\
& |b_2 - a_2| > \max(|-6a_3^{\text{est}}T + 12a_4^{\text{est}}T^2|, |-6b_4^{\text{est}}T + 12b_4^{\text{est}}T^2|). \qquad (78)
\end{aligned}
$$

Hence, if the rough estimations through STFT or PFT are fairly accurate, then the only possibility of cross-terms producing impulse is, if a_4, a_3, and a_2 are sufficiently close to b_4, b_3, and b_2, respectively.

5.3 Simulation for Parameter Estimation Using GFAF

To demonstrate the effectiveness of ck-GFAF, amplitude-modulated cubic chirp x(t) is considered, which is a sum of two amplitude-modulated cubic chirps $x_1(t)$ and $x_2(t)$ given by:

$$
\begin{aligned}
x_1(t) &= \exp\left[i\pi(a_1 t + a_2 t^2 + a_3 t^3 + a_4 t^4)\right] \quad -1 \leq t < 1 \text{ (in seconds)}, \\
x_2(t) &= \exp\left[i\pi(b_1 t + b_2 t^2 + b_3 t^3 + b_4 t^4)\right] \quad -1 \leq t < 1 \text{ (in seconds)}, \qquad (79) \\
x(t) &= 2\mathrm{e}^{-0.08t} \cdot x_1(t) + 1.5\mathrm{e}^{-0.04t} \cdot x_2(t). \qquad (80)
\end{aligned}
$$

Simulations have been done to estimate the parameters of a fourth order chirp using GFAF. The GFAF technique has proven to be successful in estimating chirp parameters from signals containing multiple chirps. Here a_4, a_3, a_2 and a_1 are cubic rate, quadratic rate, chirp rate, and Doppler frequency of the first component of multicomponent cubic chirp. Similarly b_4, b_3, b_2 and b_1 are cubic rate, quadratic rate, chirp rate, and Doppler frequency of second component of multicomponent cubic chirp. In the case of multicomponent signals, a good separation of various components present in the signal in the GFAF domain is required for effective parameter estimation.

Short time Fourier transform is used to find a rough estimation of parameters of the multicomponent signal. STFT cannot provide excellent parameter estimation due to the dispersive nature of cubic chirp in the Fourier domain. Parameters estimation of a multicomponent signal is obtained by fine search or focusing near to optimum parameter of individual component in a multicomponent chirp signal. Generally, the cross-terms have a different optimum angle as compared to the optimum angle of auto-terms, so it cannot give impulse at GFAF optimum angle α and optimum λ. So the effect of cross-terms can be reduced in the GFAF domain. Conditions to avoid cross-terms are given in the previous subsection. Under such cross-terms avoiding condition, Parameter estimation of two closely spaced multicomponent cubic frequency-modulated signals is presented in Table 2. Furthermore, the signal $x_1(t)$ given by Eq. (79) is considered to analyze the effect of amplitude modulation in parameter estimation in the presence of noise. It is observed that parameter estimation fails an SNR of -5 dB.

Table 2 Parameter estimation of an amplitude-modulated chirp having multiple components

Parameter Values	Chirp parameters							
	a_1	a_2	a_3	a_4	b_1	b_2	b_3	b_4
Actual	5	5	5	1	5	5	5	2
Estimated	5	4.88	5.13	1.07	5	5.002	5.086	2.07

6 SNR Gain and Mean Error Analysis of ck-GFAF

6.1 GFAF SNR Gain Analysis

Consider a cubic chirp signal $x(t) = A \cdot \exp[i\pi(a_1 t + a_2 t^2 + a_3 t^3 + a_4 t^4)]$. The GFAF of the signal $x(t)$ is defined as:

$$\begin{aligned}
\mathrm{AF}^{G}_{x(t),\alpha,\lambda}(\tau, f) &= \int_{-\infty}^{\infty} x(t+\tau/2)x^*(t-\tau/2)K_{\alpha,\lambda}(t, f)\mathrm{d}t \\
&= |A|^2\sqrt{1-i\cot\alpha}\int_{-\infty}^{\infty}\exp\Bigg[i\pi\Bigg((4a_4\tau - f_0^3\lambda)t^3 + (3a_3\tau + f_0^2\cot\alpha)t^2 \\
&\quad + (2a_2\tau + a_4\tau^3 - 2f\,\mathrm{cosec}\alpha)t + t_0^2 f^2\cot\alpha + \lambda(t_0 f)^3 \\
&\quad + a_1\tau + \frac{a_3\tau^3}{4}\Bigg)\Bigg]\mathrm{d}t. \qquad (81)
\end{aligned}$$

The approximate analytical expression for the GFAF magnitude spectrum of a signal $x(t)$ denoted by $|\mathrm{AF}^{G}_{x(t),\alpha,\lambda}(\tau, f)|^2$, using the stationary phase approximation for unmatched cubic phase condition, where $|2a_2\tau + a_4\tau^3 - 2f\,\mathrm{cosec}(\alpha)| >> 0$ is

$$\begin{aligned}
\left|\mathrm{AF}^{G}_{x(t),\alpha,\lambda}(\tau, f)\right| \approx 2\cdot &\sqrt{\frac{|A|^4\,\mathrm{cosec}\alpha}{\sqrt{\left(3a_3\tau + f_0^2\cot\alpha\right)^2 - 6\left(4a_4\tau - f_0^3\lambda\right)\left(a_2\tau + \frac{a_4\tau^3}{2} - f\,\mathrm{cosec}\alpha\right)}}} \\
&\cos\Bigg(\frac{\pi\sqrt{\left(3a_3\tau + f_0^2\cot\alpha\right)^2 - 6\left(4a_4\tau - f_0^3\lambda\right)\left(a_2\tau + \frac{a_4\tau^3}{2} - f\,\mathrm{cosec}\alpha\right)}}{27\left(4a_4\tau - f_0^3\lambda\right)^2} \\
&\cdot\left[12\left(4a_4\tau - f_0^3\lambda\right)\left(a_2\tau + \frac{a_4\tau^3}{2} - f\,\mathrm{cosec}\alpha\right) - 2\left(3a_3\tau + f_0^2\cot\alpha\right)^2\right] - \frac{\pi}{4}\Bigg).
\end{aligned}$$

At GFAF-matched condition, ($4a_4\tau = f_0^3\lambda$ and $3a_3\tau = -f_0^2\cot\alpha$) we get an impulse at $f = a_2\tau\sin\alpha + \frac{a_4\tau^3}{2}\sin\alpha$ with area $|A|^2||A_\alpha|$, where $|A_\alpha|$ is the amplitude of GTFT kernel.

SNR gain analysis at GFAF-matched condition has been derived as follows, considering input signal $x(t)$ corrupted by additive white Gaussian noise $n(t)$ of variance

σ_n^2. SNR of the output signal $y(t) = x(t) + n(t)$ is given by [3,21,46,55]

$$\mathrm{SNR}^{\mathrm{GFAF}} = \frac{|\mathrm{AF}^{G}_{x(t),\alpha,\lambda}(\tau, f)|^2}{\mathrm{var}\left[|\mathrm{AF}^{G}_{y(t),\alpha,\lambda}(\tau, f)|\right]}, \tag{82}$$

where $|\mathrm{AF}^{G}_{x(t),\alpha,\lambda}(\tau, f)|$ is peak modulus of GFAF of the signal $x(t)$, var represents the variance operator, and var $\left[|\mathrm{AF}^{G}_{y(t),\alpha,\lambda}(\tau, f)|\right]$ is variance of the peak of the modulus of GFAF of received signal $y(t)$. It can be expressed as

$$\mathrm{var}\left[|\mathrm{AF}^{G}_{y(t),\alpha,\lambda}(\tau, f)|\right] = \mathbb{E}\left[\left|\mathrm{AF}^{G}_{y(t),\alpha,\lambda}(\tau, f)\right|^2\right] - \mathbb{E}^2\left[\left|\mathrm{AF}^{G}_{y(t),\alpha,\lambda}(\tau, f)\right|\right]. \tag{83}$$

Since the signal and noise are uncorrelated and noise is having zero mean,

$$\begin{aligned}
&\mathbb{E}\left[\left|\mathrm{AF}^{G}_{y(t),\alpha,\lambda}(\tau, f)\right|\right] \\
&\quad = \int_{-\infty}^{+\infty} \mathbb{E}\left(\left[x\left(t+\frac{\tau}{2}\right) + n\left(t+\frac{\tau}{2}\right)\right]\left[x^*\left(t-\frac{\tau}{2}\right) + n^*\left(t-\frac{\tau}{2}\right)\right]\right) \\
&\qquad K_{\alpha,\lambda}(t, f)\mathrm{d}t. \\
&\therefore \mathbb{E}\left[\left|\mathrm{AF}^{G}_{y(t),\alpha,\lambda}(\tau, f)\right|\right] = |A|^2|A_\alpha|T^2 + \sigma_n^2|A_\alpha|T,
\end{aligned} \tag{84}$$

where T is the time duration of $x(t)$.
Similarly,

$$\begin{aligned}
\mathbb{E}\left[\left|\mathrm{AF}^{G}_{y(t),\alpha,\lambda}(\tau, f)\right|^2\right] &= \int\int_{-\infty}^{+\infty} \mathbb{E}\left(\left[x\left(t_1+\frac{\tau}{2}\right) + n\left(t_1+\frac{\tau}{2}\right)\right]\right. \\
&\quad \left[x^*\left(t_1-\frac{\tau}{2}\right) + n^*\left(t_1-\frac{\tau}{2}\right)\right] \\
&\quad \left.\left[x^*\left(t_2+\frac{\tau}{2}\right) + n^*\left(t_2+\frac{\tau}{2}\right)\right]\left[x\left(t_2-\frac{\tau}{2}\right) + n\left(t_2-\frac{\tau}{2}\right)\right]\right) \\
&\quad K_{\alpha,\lambda}(t_1, f)K^*_{\alpha,\lambda}(t_2, f)\mathrm{d}t_1\mathrm{d}t_2. \\
\therefore \mathbb{E}\left[\left|\mathrm{AF}^{G}_{y(t),\alpha,\lambda}(\tau, f)\right|^2\right] &= |A_\alpha|^2\left[|A|^4T^4 + 2T^2\sigma_n^4 + 4T^3|A|^2\sigma_n^2\right].
\end{aligned} \tag{85}$$

Hence, variance is given by

$$\mathrm{var}|\mathrm{AF}^{G}_{y(t),\alpha,\lambda}(\tau, f)| = |A_\alpha|^2\left[\sigma_n^4T^2 + 2T^3|A|^2\sigma_n^2\right]. \tag{86}$$

Therefore, GFAF SNR and SNR gain are given by

$$\mathrm{SNR}^{\mathrm{GFAF}} = \frac{|A_\alpha|^2|A|^4T^4}{|A_\alpha|^2\left[\sigma_n^4T^2 + 2T^3|A|^2\sigma_n^2\right]} = \frac{T^2\mathrm{SNR}_t^2}{2T\mathrm{SNR}_\mathrm{t} + 1}, \tag{87}$$

$$\frac{\mathrm{SNR}^{\mathrm{GFAF}}}{\mathrm{SNR}_\mathrm{t}} \approx \frac{T}{2}, \tag{88}$$

where SNR_t is input SNR, defined as A^2/σ_n^2. In discrete case, SNR gain is given by

$$\frac{\mathrm{SNR}^{\mathrm{GFAF,discrete}}}{\mathrm{SNR}_\mathrm{t}} \approx D\frac{N}{K}, \tag{89}$$

where D is a constant, K is the number of components, and N is the number of samples during signal pulse time T.

6.1.1 SNR Gain Simulation

Consider a signal for SNR gain and mean error under different SNR conditions (Monte Carlo simulation) as

$$s(t) = x_1(t) + x_2(t) + n(t), \tag{90}$$

where $n(t)$ is an additive white Gaussian noise (AWGN), $x_1(t)$ and $x_2(t)$ are fourth-order chirp signals defined by

$$\begin{aligned} x_1(t) &= \exp\left(i\pi(4t^4 + 4t^3 + 5t^2 + 4t)\right), \qquad -1 \le t < 1 \text{ (in seconds)},\\ x_2(t) &= \exp\left(i\pi(20t^4 + 15t^3 + 10t^2 + 5t)\right), \qquad -1 \le t < 1 \text{ (in seconds)}, \end{aligned} \tag{91}$$

Monte Carlo simulations for 200 noise realizations have been performed to compare the SNR gain of GFAF and time domain-matched filtering for individual cubic chirp components $x_1(t)$ and $x_2(t)$. The search range for the quadratic rate of the kernel (λ) is considered to be (-13.4 : 0.001 : -13.42) and (19.99 : 0.001 : 20.01) for first and second component, respectively. Similarly, the search range of GTFT optimum angle (α) is considered (0.7991 : 0.001 : 0.8291) and (-0.99 : 0.001 : -1) for first and second component respectively.

As shown in Fig. 3, time domain-matched filtering gives the highest SNR in case of additive white Gaussian noise (AWGN), and it is equivalent to N_1, where N_1 is the product of the bandwidth and the pulse width. GFAF is observed to have a lesser SNR gain compared to that of time domain-matched filtering but performs better than FrFT-based AF and classical AF.

6.2 Mean Square Error Analysis Simulation

Monte Carlo simulations for 200 noise realizations has been performed to compare mean square errors in estimating cubic chirp parameters using GFAF of individual

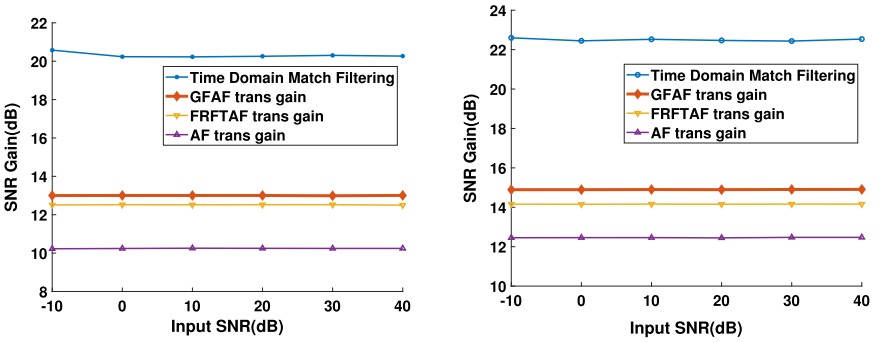

(a) SNR gain comparison of first component **(b)** SNR gain comparison of second component

Fig. 3 Monte Carlo Simulation to estimate the performance of GFAF in SNR gain

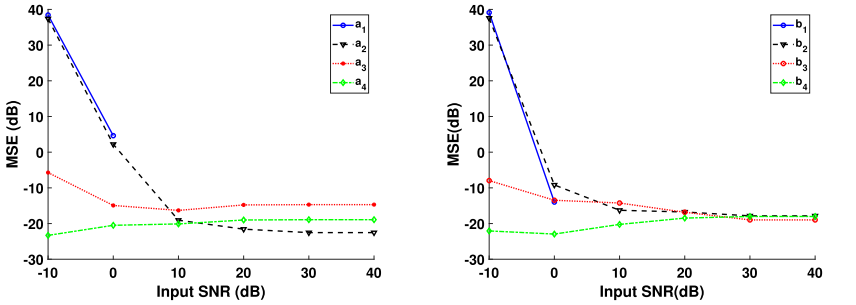

(a) MSE in parameter estimation of first component **(b)** MSE in parameter estimation of second component

Fig. 4 Monte Carlo simulation to estimate the performance of GFAF in parameter estimation

quadratic chirp components $x_1(t)$ and $x_2(t)$ as mentioned in Eq. (91). The search range of quadratic rate and GTFT optimum angle are considered similar to the search range for SNR gain analysis for first and second components. Figure 4a shows the MSE in the estimation of first component $x_1(t)$ parameters in the presence of second component $x_2(t)$ and AWGN noise $n(t)$. Similarly Fig. 4b shows the MSE in the estimation of second component $x_2(t)$ parameters in presence of first component $x_1(t)$ and AWGN noise $n(t)$. Finally, as shown in Fig. 4 as SNR increases, GFAF does better at parameter estimation and has lesser MSE in the estimations.

GFAF-based parameter estimation is a nonlinear transform and produces cross-terms during multicomponent chirp signals. So it will not work satisfactorily at low SNR condition in case of multicomponent chirp signals. Furthermore, reduction in cross-terms can be explored by using the product of different lag GFAF or product-GFAF during multicomponent polynomial phase signal analysis. Some smoothing filter can be explored to remove cross-terms of GFAF for multicomponent weak or low SNR signals detection.

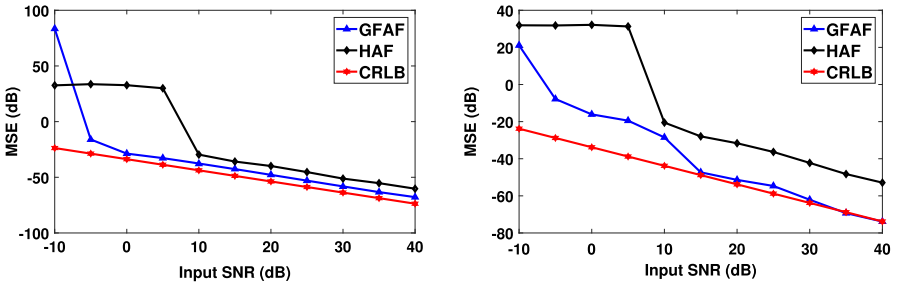

(a) MSE in a_3 parameter estimation **(b)** MSE in a_4 parameter estimation

Fig. 5 Comparison of MSE in parameter estimation with different transforms

6.3 Comparison of MSE in Parameter Estimation with Different Transforms

The GFAF method is compared with different estimators such as HAF and Cramer–Rao lower bound (CRLB) [4,38]. Here, we consider a chirp signal $x(t)$ given by

$$x(t) = \exp\left(i\pi(20t^4 + 15t^3 + 10t^2 + 5t)\right), -1 \leq t < 1 \text{ (in seconds)}. \tag{92}$$

Monte Carlo simulations have been performed for 100 iterations to obtain the MSE in the estimation of the parameters a_3 and a_4 in case of a single component chirp signal. The results are as shown in Fig. 5. Each phase differentiation or correlation increases the SNR threshold by approximately 6 dB [4]. GFAF performs only one de-chirping or phase differentiation for estimating the fourth-order phase coefficient a_4. In contrast, HAF performs multiple de-chirping to estimate the fourth-order phase coefficient. As shown in Fig. 5, HAF follows CRLB after 12 dB input SNR, whereas GFAF follows CRLB at approximately 6 dB input SNR. So HAF has a higher SNR threshold then GFAF for estimating chirp parameters. As shown in Fig. 5b, GFAF performs better than HAF transform for estimating the higher order phase coefficient a_4.

Error propagation is happening due to the correlation operation. GFAF uses lesser correlation operation as compared to HAF for estimating cubic chirp. As shown in Fig. 5a, error propagation in GFAF from higher- to lower-order phase coefficient a_3 is very less as compared to HAF, due to a single de-chirping operation. Also, GFAF performs better than HAF transform for estimating the lower-order phase coefficient a_3. As opposite to HAF, GFAF estimates more parameters of cubic chirp at once. Hence, error propagation is less in GFAF as compared to HAF. As shown in both the diagrams in Fig. 5, at higher SNR, the GFAF-estimated parameters follow CRLB-estimated parameters.

A combination of correlation and higher-order GTFT kernel in GFAF can be used to analyze any frequency-modulated chirp. As the number of correlations increases, the SNR threshold increases, and as the order of GTFT kernel increases, computational complexity increases. Thus, GFAF gives the flexibility to choose the number of correlations and order of GTFT kernel based on SNR threshold and computational

complexity requirement for analyzing any higher-order chirp signals. These properties make GFAF superior to other transforms.

In the case of higher-order chirp signals with low SNR and very high phase order, GFAF needs to use multiple correlators to reduce computational complexity during parameter estimation. Each correlation increases the SNR threshold by approximately 6 dB and also increases cross-terms. In such a condition, GFAF cannot estimate the parameter of low-SNR, higher-order chirp signals.

6.4 Error Propagation Analysis

This section presents error propagation analysis for estimating single component cubic chirp parameter using GFAF. Cubic chirp is considered as defined in Sect. 5.2.1.

Consider α_{opt}, λ_{opt}, τ_{opt} and f_{opt} be the optimum values obtained at matched condition. Let $\delta\alpha$, $\delta\lambda$ and δf be estimation errors in calculating α_{opt}, λ_{opt} and f_{opt}, respectively. We find error in a_4, a_3, a_2 and a_1, i.e., δa_4, δa_3, δa_2 and δa_1 in terms of $\delta\alpha$, $\delta\lambda$ and δf. For simplicity of analysis, we assume that the estimation error in calculating τ_{opt} is negligible. Thus, $\tau = \tau_{\text{opt}}$. For readability, we denote λ_{opt}, α_{opt}, f_{opt} by λ, α, f, respectively.

Similar to the method in [28], $\delta\alpha$, $\delta\lambda$ and δf are considered uncorrelated Gaussian random variables $N(0, \sigma_\alpha^2)$, $N(0, \sigma_\lambda^2)$ and $N(0, \sigma_f^2)$, respectively. Also let $\mathbb{E}[\delta\alpha \cdot \delta\lambda] = \sigma_{\alpha,\lambda}^2$, $\mathbb{E}[\delta\alpha \cdot \delta f] = \sigma_{\alpha,f}^2$ and $\mathbb{E}[\delta\lambda \cdot \delta f] = \sigma_{\lambda,f}^2$.

From the matched conditions in Eqs. (62–64), we can calculate the error variance in a_4, a_3, a_2 and a_1. Using the cubic matched condition in Eq. (62), we get:

$$a_4 = \frac{f_o^3 \lambda}{4\tau},$$

$$\delta a_4 = \frac{f_o^3 \cdot \delta\lambda}{4\tau}, \tag{93}$$

$$\text{var}(\delta a_4) = \frac{f_o^6 \cdot \sigma_\lambda^2}{(4\tau)^2}. \tag{94}$$

Substituting the value of a_4 from Eq. (62) in quadratic matched condition of Eq. (63), we obtain:

$$a_3 = -\frac{f_o^2 \cot\alpha}{3\tau} + \frac{f_o^3 \lambda}{2}, \tag{95}$$

$$\delta a_3 = \frac{f_o^3 \cdot \delta\lambda}{2} + \frac{f_o^2 \text{cosec}^2\alpha \cdot \delta\alpha}{3\tau}, \tag{96}$$

$$\text{var}(\delta a_3) = \frac{f_o^6 \cdot \sigma_\lambda^2}{4} + \frac{f_o^4 \text{cosec}^4\alpha \cdot \sigma_\alpha^2}{(3\tau)^2} + \frac{f_o^5 \text{cosec}^2\alpha \cdot \sigma_{\alpha,\lambda}^2}{3\tau}. \tag{97}$$

Substituting the value of a_4 from Eq. (62) and a_3 from Eq. (63) in the linear matched condition of Eq. (64), we get:-

$$a_2 = \frac{f\,\mathrm{cosec}\alpha}{\tau} - \frac{f_o^2\cot\alpha}{2} + \frac{f_o^3\lambda\tau}{4}, \tag{98}$$

$$\delta a_2 = \frac{f\,\mathrm{cosec}\alpha\cdot\cot\alpha\cdot\delta\alpha}{\tau} + \frac{f_o^2\mathrm{cosec}^2\alpha\cdot\delta\alpha}{2} + \frac{f_o^3\tau\cdot\delta\lambda}{4} + \frac{\mathrm{cosec}\alpha\cdot\delta f}{\tau}, \tag{99}$$

$$\begin{aligned}\mathrm{var}(\delta a_2) = {} & \frac{f^2\mathrm{cosec}^2\alpha\cdot\cot^2\alpha\cdot\sigma_\alpha^2}{\tau^2} + \frac{f_o^4\mathrm{cosec}^4\alpha\cdot\sigma_\alpha^2}{4} + \frac{f_o^6\tau^2\cdot\sigma_\lambda^2}{16} \\ & + \frac{\mathrm{cosec}^2\alpha\cdot\sigma_f^2}{\tau^2} + \frac{ff_o^2\mathrm{cosec}^3\alpha\cdot\cot\alpha\cdot\sigma_\alpha^2}{\tau} + \frac{ff_o^3\mathrm{cosec}\alpha\cdot\cot\alpha\cdot\sigma_{\alpha,\lambda}^2}{2} \\ & + \frac{2f\,\mathrm{cosec}^2\alpha\cdot\cot\alpha\cdot\sigma_{\alpha,f}^2}{\tau^2} + \frac{f_o^5\tau\,\mathrm{cosec}^2\alpha\cdot\sigma_{\alpha,\lambda}^2}{4} + \frac{f_o^2\mathrm{cosec}^3\alpha\cdot\sigma_{\alpha,f}^2}{\tau} \\ & + \frac{f_o^3\mathrm{cosec}\alpha\cdot\sigma_{\lambda,f}^2}{2}.\end{aligned} \tag{100}$$

To get a_1, we multiply the original signal with the conjugate of the estimated signal as mentioned in 5.2.1. Taking the Fourier transform of the received signal, let f' be the frequency corresponding to the maxima. Then $a_1 = 2f'$ when estimation error in a_2, a_3 and a_4 are neglected.

Let δa_1 correspond to the error in a_1.

$$a_1 - 2f' = \delta a_1, \tag{101}$$

$$f' = \mathrm{argmax}_f\left[\int_{-T}^{T}\exp[i\pi(\delta a_4 t^4 + \delta a_3 t^3 + \delta a_2 t^2 + (a_1 - 2f)t)]\mathrm{d}t\right], \tag{102}$$

where $\mathrm{argmax_f}$ denotes the maximum of the argument over all f. Since the powers of estimation error in the parameters will be very small for the high SNR regime, i.e., $\delta a_4 T^4 + \delta a_3 T^3 + \delta a_2 T^2 + (a_1 - 2f)T \ll 1$, we use the approximation $\mathrm{e}^x \approx 1 + x + \frac{x^2}{2}$.

$$\begin{aligned}f' \approx \mathrm{argmax}_f\Bigg[\int_{-T}^{T}\Bigg(1 + i\pi[\delta a_4 t^4 + \delta a_3 t^3 + \delta a_2 t^2 + (a_1 - 2f)t] \\ + \frac{[i\pi(\delta a_4 t^4 + \delta a_3 t^3 + \delta a_2 t^2 + (a_1 - 2f)t)]^2}{2}\Bigg)\mathrm{d}t\Bigg],\end{aligned} \tag{103}$$

$$f' = \mathrm{argmax}_f\left[K + \left(\frac{T^3(a_1 - 2f)^2}{3} + \frac{2T^5\delta a_3(a_1 - 2f)}{5}\right)\right], \tag{104}$$

where

$$K = \int_{-T}^{T} \left(1 + i\pi(\delta a_4 t^4 + \delta a_3 t^3 + \delta a_2 t^2) + \frac{[i\pi(\delta a_4 t^4 + \delta a_3 t^3 + \delta a_2 t^2)]^2}{2}\right) \mathrm{d}t. \tag{105}$$

Thus, K is independent of f. To maximize above expression, optimal $f = f'$ is found at the critical point. On differentiating Eq. (104) with respect to f and equating the result to 0, we obtain:

$$f' = \frac{1}{2}\left[a_1 - \frac{3T^2 \cdot \delta a_3}{5}\right], \tag{106}$$

Further, using Eq. (101), we get:

$$\delta a_1 = \frac{3T^2 \cdot \delta a_3}{5}, \tag{107}$$

$$\mathrm{var}(\delta a_1) = \frac{9T^4 \cdot \mathrm{var}(\delta a_3)}{25}. \tag{108}$$

Writing $T = f_s N$, we note that the relation between $\mathrm{var}(\delta a_1)$ and $\mathrm{var}(\delta a_3)$ is consistent with the CRLB bounds for fourth-order chirp [32].

Thus, from Eq. (108), the estimation error in a_1, i.e., δa_1 is majorly dependent on the estimation error in a_3, i.e., δa_3. It will also depend on estimation errors in δa_2 and δa_4 (if we consider higher-order terms in the series expansion of e^x). However, the propagation of error in δa_1 by δa_2 and δa_4 will be much smaller than the error propagation by δa_3. Note that this result will also hold if estimation error in τ_{opt} is considered.

At higher values of SNR, the x^2 term can also be neglected and thus the error in a_1 becomes almost negligible. This can be observed in Fig. 4 at higher values of SNR.

7 Real Multicomponent Bat Echolocation Signal Analysis

The real echolocation signal of a large brown bat is considered to estimate its parameters. It is a multicomponent chirp signal with a sampling frequency of 142, 000 Hz with 400 samples. TFDs of adaptive fractional spectrogram (AFS) are demonstrated in Fig. 6a for better illustration of the four components of bat signal. Figure 6b, d represent 3D plot and shift-amplitude distribution of GFAF for bat signal, respectively. As shown in Fig. 6c, four impulse or peaks are visible in the frequency-amplitude distribution of the GFAF plot corresponding to the four components of the bat signal. As mentioned in [6], this signal contains four components at different time-intervals, whose parameters are reported in Tables 3 and 4. The parameters of this signal are estimated by focusing on four components of a multicomponent bat signal using the algorithm mentioned in Sect. 5.2.1. As shown in Table 3, the signal is considered to

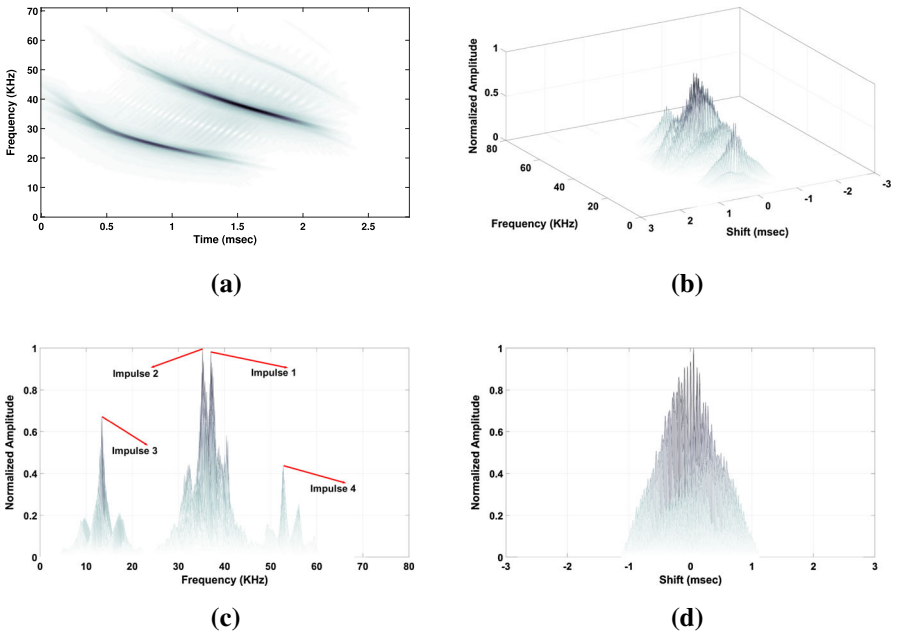

Fig. 6 Spectrogram view of real bat echolocation signal using different TFDs. **a** AFS, **b** 3D plot of GFAF, **c** frequency- amplitude distribution of GFAF, **d** shift-amplitude distribution of GFAF

Table 3 Parameter estimation of a bat echolocation signal having multiple components of 3rd order

Signal	Sample range	Estimated parameters		
		a_3	a_2	a_1
1st component	1:150	9.9467×10^9	-3.5058×10^7	8.7093×10^4
2nd component	121:280	2.5174×10^9	-1.8906×10^7	9.7625×10^4
3rd component	226:385	-8.7099×10^9	-5.6132×10^6	7.2775×10^4
4th component	141:280	4.1639×10^9	-2.0173×10^7	9.3314×10^4

be a chirp of third order, and FrFT-based AF is applied to estimate its parameters. As shown in Table 4, the signal is considered to be a chirp of fourth order, and ck-GFAF is applied to estimate its parameters up to fourth order. For both cases, the estimated parameters for different components until third order are found to be similar.

8 Sigmoid-Based GFAF

Similar to fractional Fourier transform-based AF [18], we propose sigmoid-based GFAF and GWVD for the algorithm to work under non-Gaussian noise. These sigmoid-based transforms do not require any prior knowledge of impulse noise and have been shown to be capable of reducing impulse noise in parameter estimation in

Table 4 Parameter estimation of a bat echolocation signal having multiple components of 4th order

Signal	Sample range	Estimated parameters			
		a_4	a_3	a_2	a_1
1st component	1:150	-5.0493×10^{10}	1.1832×10^{10}	-3.8411×10^{7}	8.8987×10^{4}
2nd component	121:280	8.9772×10^{10}	2.7342×10^{9}	-1.9232×10^{7}	9.7625×10^{4}
3rd component	226:385	6.3435×10^{12}	-1.3906×10^{10}	-5.7777×10^{6}	7.2775×10^{4}
4th component	141:280	-3.7566×10^{11}	4.427×10^{9}	-2.0173×10^{7}	9.3314×10^{4}

fractional Fourier transform, and fractional Fourier transform-based ambiguity function [18,19].
For a given signal $x(t)$ with finite L^2 norm:

– The proposed sigmoid-based GFAF, $\mathrm{AF}^{S}_{x(t),\alpha,\lambda}(\tau, f)$ is defined as

$$\mathrm{AF}^{S}_{x(t),\alpha,\lambda}(\tau, f) = \int_{-\infty}^{\infty} \mathrm{sigmoid}[x(t+\tau/2)]\mathrm{sigmoid}[x^*(t-\tau/2)]K_{\alpha,\lambda}(t, f)\mathrm{d}t. \tag{109}$$

– The proposed sigmoid-based GFWVD, $WDF^{S}_{x(t),\alpha,\lambda}(t, f)$ is defined as

$$WDF^{S}_{x(t),\alpha,\lambda}(t, f) = \int_{-\infty}^{\infty} \mathrm{sigmoid}[x(t+\tau/2)]\mathrm{sigmoid}[x^*(t-\tau/2)]K_{\alpha,\lambda}(\tau, f)\mathrm{d}\tau, \tag{110}$$

where $\mathrm{sigmoid}[x(t)] = \frac{2}{1+\exp[-x(t)]} - 1$. However, this paper is limited to GFAF for Gaussian noise, and the extensive study of these transforms under non-Gaussian noise conditions can be considered in the future.

9 Conclusion

A new kind of AF- and WDF-based on GTFT to estimate the parameter of higher-order chirp signals, and to analyze higher-order radar waveforms is proposed. GFAF can be used to analyze various waveform properties of higher-order chirp signals for its suitability as a radar waveform. GFAF and GFWVD can be used to estimate a large variety of multicomponent higher-order chirp signals by choosing the appropriate $h(\cdot)$ function in GTFT kernel. GFAF follows the property of index additivity of angle (similar to FrFT); hence, GFAF is computationally efficient. The computational complexity of GFAF is lesser than generalized CPF, maximum likelihood, and QML estimator for estimating higher-order chirp parameters. GFAF is computationally efficient as compared to the GTFT for estimating the same higher-order chirp. However, as the chirp order increases, the computational complexity for parameter estimation using GFAF increases. In such cases, a combination of correlation and higher-order GTFT kernel

in GFAF can be used to analyze any higher-order chirp with reasonable computational complexity. SNR gain of ck-GFAF for multicomponent cubic frequency-modulated signal is less than time domain-matched filter but is more than that of FrFT-based AF and classical AF. At higher SNR, GFAF-estimated parameters follow CRLB-estimated parameters. GFAF can provide better SNR threshold as compared to HAF, and other multi-lag phase differentiation transforms due to the use of a single de-chirping operation. Ck-GFAF is capable of estimating fourth-order parameters of all the four components of the real multicomponent bat signal, and it is comparable with estimated parameters of FrFT-based AF. Parameter estimation and waveform analysis of chirp signal using GFAF and GFWVD can be used in applications such as radar, sonar, and biomedical signal processing.

In the future, GFAF applications on SAR ground moving target detection and imaging will be explored further and compared with different techniques. The possibility of using GFAF for analyzing properties of different waveforms such as hyperbolic chirp, sinusoidal frequency-modulated waveform, etc., can be explored. Product GFAF with different lags can be explored to reduce the effect of cross-terms during multicomponent signal analysis. The possibility of using a smoothing filter can be explored to remove cross-terms of GFAF during multicomponent analysis. Sigmoid-based GFAF and GWVD can be used for parameter estimation of higher-order chirps under non-Gaussian noise conditions.

Acknowledgements The authors would like to thank the DRDO, Ministry of Defence, Govt. of India, for sponsorship of Peeyush Sahay, Sc 'E' (Ph.D. student) under the R&D scheme, at IIT Bombay. The authors would like to thank Mr. Adway Girish, Shubham Kar, Shaan Ul Haque, Parth Dodhia, and Titas Chakraborty (B.Tech, IIT Bombay) for improving the quality of the paper. The authors also wish to thank Curtis Condon, Ken White, and Al Feng of the Beckman Institute of the University of Illinois for the bat data and for permission to use it in this paper.

References

1. L.B. Almeida, The fractional Fourier transform and time-frequency representations. IEEE Trans. Signal Process. **42**(11), 3084–3091 (1994)
2. X. Bai, R. Tao, L.J. Liu, J. Zhao, Autofocusing of SAR images using STFRFT-based preprocessing. Electron. Lett. **48**(25), 1622–1624 (2012)
3. S. Barbarossa, V. Petrone, Analysis of polynomial-phase signals by the integrated generalized ambiguity function. IEEE Trans. Signal Process. **45**(2), 316–327 (1997)
4. B. Boashash, *Time-Frequency Signal Analysis and Processing: A Comprehensive Reference* (Academic Press, Orlando, 2015)
5. R. Cao, M. Li, L. Zuo, Z. Wang, Y. Lu, A new method for parameter estimation of high-order polynomial-phase signals. Sig. Process. **142**, 212–222 (2018)
6. C. Capus, K. Brown, Short-time fractional Fourier methods for the time-frequency representation of chirp signals. J. Acoust. Soc. Am. **113**(6), 3253–3263 (2003)
7. T.-W. Che, B.-Z. Li, T.-Z. Xu, The ambiguity function associated with the linear canonical transform. EURASIP J. Adv. Signal Process. **2012**(1), 1–14 (2012)
8. V.C. Chen, *The Micro-Doppler Effect in Radar* (Artech House, Norwood, 2019)
9. V.C. Chen, D. Tahmoush, W.J. Miceli, *Radar Micro-Doppler Signatures: Processing and Applications* (Institution of Engineering and Technology, Herts, 2014)
10. X. Chen, Y. Huang, N. Liu, J. Guan, Y. He, Radon-fractional ambiguity function-based detection method of low-observable maneuvering target. IEEE Trans. Aerosp. Electron. Syst. **51**(2), 815–833 (2015)

11. I.G. Cumming, F.H. Wong, *Digital Processing of Synthetic Aperture Radar Data* (Artech House, Norwood, 2005)
12. I. Djurović, M. Simeunović, Review of the quasi-maximum likelihood estimator for polynomial phase signals. Digit. Signal Proc. **72**, 59–74 (2018)
13. I. Djurović, M. Simeunović, P. Wang, Cubic phase function: a simple solution to polynomial phase signal analysis. Sig. Process. **135**, 48–66 (2017)
14. I. Djurovic, T. Thayaparan, L. Stankovic, SAR imaging of moving targets using polynomial Fourier transform. IET Signal Proc. **2**(3), 237–246 (2008)
15. M. El-Mashed, O. Zahran, M.I. Dessouky, M. El-Kordy, F.A. El-Samie, Synthetic aperture radar imaging with fractional Fourier transform and channel equalization. Digit. Signal Proc. **23**(1), 151–175 (2013)
16. P. Huang, G. Liao, Z. Yang, X. Xia, J. Ma, X. Zhang, A fast SAR imaging method for ground moving target using a second-order WVD transform. IEEE Trans. Geosci. Remote Sens. **54**(4), 1940–1956 (2016)
17. P. Huang, G. Liao, Z. Yang, X.G. Xia, J. Ma, J. Zheng, Ground maneuvering target imaging and high-order motion parameter estimation based on second-order keystone and generalized Hough-HAF transform. IEEE Trans. Geosci. Remote Sens. **55**(1), 320–335 (2017)
18. L. Li, T. Qiu, A novel phase parameter estimation method of quadratic FM signal based on Sigmoid fractional ambiguity function in impulsive noise environment. AEU-Int. J. Electron. Commun. **93**, 268–276 (2018)
19. L. Li, N.H. Younan, X. Shi, Joint estimation of Doppler stretch and time delay of wideband echoes for LFM pulse radar based on Sigmoid-FRFT transform under the impulsive noise environment. Electronics **8**(2), 121 (2019)
20. X. Li, G. Bi, S. Stankovic, A.M. Zoubir, Local polynomial Fourier transform: a review on recent developments and applications. Sig. Process. **91**(6), 1370–1393 (2011)
21. J.G. Liu, B.C. Yuan, The analysis and simulation of the detectors based on FRFT statistic performance, in *2008 Asia Simulation Conference-7th International Conference on System Simulation and Scientific Computing* (2008), pp. 1543–1548
22. S. Liu, Y. Ma, T. Shan, Segmented discrete polynomial-phase transform with coprime sampling. J. Eng. **2019**(19), 5619–5621 (2019)
23. S. Liu, T. Shan, R. Tao, Y.D. Zhang, G. Zhang, F. Zhang, Y. Wang, Sparse discrete fractional Fourier transform and its applications. IEEE Trans. Signal Process. **62**(24), 6582–6595 (2014)
24. S. Liu, T. Shan, Y.D. Zhang, R. Tao, Y. Feng, A fast algorithm for multi-component LFM signal analysis exploiting segmented DPT and SDFrFT, in *2015 IEEE Radar Conference (RadarCon)* (2015), pp. 1139–1143
25. S. Liu, Y.D. Zhang, T. Shan, Detection of weak astronomical signals with frequency-hopping interference suppression. Digit. Signal Proc. **72**, 1–8 (2018)
26. N. Nedić, D. Pršić, C. Fragassa, V. Stojanović, A. Pavlovic, Simulation of hydraulic check valve for forestry equipment. Int. J. Heavy Veh. Syst. **24**(3), 260–276 (2017)
27. N. Nedic, V. Stojanovic, V. Djordjevic, Optimal control of hydraulically driven parallel robot platform based on firefly algorithm. Nonlinear Dyn. **82**(3), 1457–1473 (2015)
28. X. Ning, L. Guo, X. Sha, Joint time delay and frequency offset estimation based on fractional Fourier transform, in *2012 International Conference on ICT Convergence (ICTC)* (2012), pp. 318–322
29. H.M. Ozaktas, O. Arikan, M.A. Kutay, G. Bozdagt, Digital computation of the fractional Fourier transform. IEEE Trans. Signal Process. **44**(9), 2141–2150 (1996)
30. V. Popović, I. Djurović, L. Stanković, T. Thayaparan, M. Daković, Autofocusing of SAR images based on parameters estimated from the PHAF. Sig. Process. **90**(5), 1382–1391 (2010)
31. T.S. Qiu, L. Li, A novel joint parameter estimation method based on fractional ambiguity function in bistatic multiple-input multiple-output radar system. Comput. Electr. Eng. **39**(4), 1248–1259 (2013)
32. B. Ristic, B. Boashash, Comments on "The Cramer–Rao lower bounds for signals with constant amplitude and polynomial phase". IEEE Trans. Signal Process. **46**(6), 1708–1709 (1998)
33. B.Z.L. Rui-Feng Bai, Q.Y. Cheng, Wigner–Ville distribution associated with the linear canonical transform. J. Appl. Math. **2012**, 1–14 (2012)
34. S. Sahay, D. Pande, N. Wing, V. Gadre, P. Sohani, A novel generalized time-frequency transform inspired by the fractional Fourier transform for higher order chirps, in *International Conference on Signal Processing and Communications (SPCOM)* (2012), pp. 1–5

35. S.B. Sahay, Parameter estimation of chirp signals. Ph.D. thesis, Department of Electrical Engineering, IIT Bombay, Mumbai, India (2015)
36. S.B. Sahay, T. Meghasyam, R.K. Roy, G. Pooniwala, S. Chilamkurthy, V. Gadre, Parameter estimation of linear and quadratic chirps by employing the fractional Fourier transform and a generalized time frequency transform. Sadhana **40**(4), 1049–1075 (2015)
37. E. Sejdić, I. Djurović, L. Stanković, Fractional Fourier transform as a signal processing tool: an overview of recent developments. Sig. Process. **91**(6), 1351–1369 (2011)
38. M. Simeunovic, I. Djurovic, CPF-HAF estimator of polynomial-phase signals. Electron. Lett. **47**(17), 965–966 (2011)
39. M. Simeunović, I. Djurović, A method for efficient maximization of PPS estimation functions. Digit. Signal Proc. **84**, 38–45 (2019)
40. Y.E. Song, C. Wang, P. Shi, Algorithm based on the linear canonical transform for QFM signal parameters estimation. IET Signal Proc. **10**(3), 318–324 (2016)
41. Y.E. Song, X.Y. Zhang, C.H. Shang, H.X. Bu, X.Y. Wang, The Wigner–Ville distribution based on the linear canonical transform and its applications for QFM signal parameters estimation. J. Appl. Math. 1–8 (2014)
42. L. Stankovic, M. Dakovic, T. Thayaparan, *Time-Frequency Signal Analysis with Applications* (Artech house, Norwood, 2014)
43. V. Stojanovic, V. Filipovic, Adaptive input design for identification of output error model with constrained output. Circuits Syst Signal Process **33**(1), 97–113 (2014)
44. V. Stojanovic, N. Nedic, A nature inspired parameter tuning approach to cascade control for hydraulically driven parallel robot platform. J. Optim. Theory Appl. **168**(1), 332–347 (2016)
45. V. Stojanovic, N. Nedic, Robust Kalman filtering for nonlinear multivariable stochastic systems in the presence of non-Gaussian noise. Int. J. Robust Nonlinear Control **26**(3), 445–460 (2016)
46. R. Tao, X.M. Li, Y.L. Li, Y. Wang, Time-delay estimation of chirp signals in the fractional Fourier domain. IEEE Trans. Signal Process. **57**(7), 2852–2855 (2009)
47. R. Tao, Y.L. Li, Y. Wang, Short-time fractional Fourier transform and its applications. IEEE Trans. Signal Process. **58**(5), 2568–2580 (2010)
48. R. Tao, Y.E. Song, Z.J. Wang, Y. Wang, Ambiguity function based on the linear canonical transform. IET Signal Proc. **6**(6), 568–576 (2012)
49. Z. Xinghao, T. Ran, D. Bing, Practical normalization methods in the digital computation of the fractional Fourier transform, in *Proceedings of 7th International Conference on Signal Processing* (2004), pp. 105–108
50. Y. Yang, Z. Peng, X. Dong, W. Zhang, G. Meng, General parameterized time-frequency transform. IEEE Trans. Signal Process. **62**(11), 2751–2764 (2014)
51. Y. Yang, Z. Peng, W. Zhang, G. Meng, Parameterised time-frequency analysis methods and their engineering applications: a review of recent advances. Mech. Syst. Signal Process. **119**, 182–221 (2019)
52. Y. Yang, W. Zhang, Z. Peng, G. Meng, Multicomponent signal analysis based on polynomial chirplet transform. IEEE Trans. Ind. Electron. **60**(9), 3948–3956 (2013)
53. Z. Zhang, M. Luo, New integral transforms for generalizing the Wigner distribution and ambiguity function. IEEE Signal Process. Lett. **22**(4), 460–464 (2015)
54. Z.C. Zhang, Novel Wigner distribution and ambiguity function associated with the linear canonical transform. Optik Int. J. Light Electron Opt. **127**(12), 4995–5012 (2016)
55. J.D. Zhu, J. Li, X.D. Gao, L.B. Ye, H.Y. Dai, Adaptive threshold detection and estimation of linear frequency-modulated continuous-wave signals based on periodic fractional Fourier transform. Circuits Syst. Signal Process. **35**(7), 2502–2517 (2016)
56. L. Zuo, M. Li, Z. Liu, L. Ma, A high-resolution time-frequency rate representation and the cross-term suppression. IEEE Trans. Signal Process. **64**(10), 2463–2474 (2016)

Affiliations

Peeyush Sahay[1] · Izaz Ahamed Shaik Rasheed[1] · Pranav Kulkarni[1] · Shubham Anand Jain[1] · Ameya Anjarlekar[1] · P. Radhakrishna[2] · Vikram M. Gadre[1]

✉ Peeyush Sahay
sahay.peeyush@gmail.com

Izaz Ahamed Shaik Rasheed
izazahamed.babji@gmail.com

Pranav Kulkarni
pranav.dk212@gmail.com

Shubham Anand Jain
shubhamjainiitb@gmail.com

Ameya Anjarlekar
ameyanjarlekar@gmail.com

P. Radhakrishna
prk@lrde.drdo.in

Vikram M. Gadre
vmgadre@ee.iitb.ac.in

1 Department of Electrical Engineering, Indian Institute of Technology, Bombay, Mumbai, India

2 Electronic and Radar Development Establishment, DRDO, Bangalore, India